UNIVERSIDADE DA BEIRA INTERIOR
Engenharia

Thermal Modelling and Experiments for Small Satellites

Daniel Campanudo Carvalhais

Dissertação para obtenção do Grau de Mestre em
Engenharia Aeronáutica
(Ciclo de estudos integrado)

(Versão final após defesa)

Orientador: Prof. Doutor Francisco Miguel Ribeiro Proença Brójo
Orientador: Paulo Vasconcelos Figueiredo
Co-orientador: André Gomes da Costa Guerra
Co-orientador: Miguel Sousa Machado

Covilhã, Dezembro de 2019

Dedication

Dedicated to my family.

Acknowledgments

I would like to express my gratitude to my supervisor at UBI: Professor Francisco Brójo for all the help and for being always there for me, proving me the essential to conclude my experiments.

Many thanks to my supervisor at CEiiA, Engineer Paulo Figueiredo. It was you who inspired me to complete this work, helping me and showing the right path to follow when I needed most. I always felt comfortable under your guidance. At the same time, I would like to thank CEiiA for giving me this opportunity to enrich me as a person and as a professional. Moreover, this gratitude includes CEiiA's team for helping me during my experiments.

Thank you all whom helped me during this thesis, especially huge thanks to my girlfriend Inês and all my friends Lucas, Paco, José, Paulo, Oliveira, Luís, Ruizinho, Laudino, Kikões and Tiago. More than helping me you were always supportive in getting me out of my shell.

Desertuna. All the skills, lessons taught, adventures and stepped stages I will never forget and always carry in my heart. Our story is not fully written.

Last but not least, I would like to express my gratitude to my parents, Manuel and Maria, and my sister for the unconditional support and care during this journey.

Resumo

Tem havido um crescente interesse nas missões e na obtenção de dados através da utilização de *CubeSats*. Estes, devido à sua dimensão e baixo custo têm uma grande flexibilidade em acomodar diferentes cargas úteis. No entanto, novas missões com cargas úteis e componentes altamente sensíveis à temperatura, o aumento da dissipação de energia (pela miniaturização de componentes e sistemas eletrónicos) e superfícies irradiadoras reduzidas levam a possíveis problemas térmicos. Uma das causas para a falha de um satélite em órbita são os picos de temperatura sofridos durante um ciclo orbital completo. Portanto, o projeto e o teste adequados do sistema de controlo térmico devem ser realizados, de forma a garantir a fiabilidade do satélite antes do seu lançamento de modo a reduzir a possibilidade de falha.

O 3-AMADEUS é um *CubeSat* de uma unidade que está atualmente a ser desenvolvido numa parceria entre o CEiiA e a UBI. O propósito desta missão é demonstrar que um sistema de determinação e controlo de atitude exclusivamente magnético, pode ser capaz de fornecer atitude orbital de três eixos para os nanossatélites. O presente trabalho tem como objetivo efetuar análises térmicas ao 3-AMADEUS *CubeSat* para confirmar a sua sobrevivência assim que for colocado em órbita. Para isso, é necessário analisar os principais processos de transferência de calor num satélite, condução e radiação, de forma a validar as metodologias atualmente utilizadas para as análises térmicas. Assim, com o objetivo de desenvolver modelos térmicos com maior fiabilidade, foram realizadas duas experiências em vácuo.

O primeiro teste experimental consiste num estudo da troca de calor entre duas placas de alumínio através de radiação, usando uma lâmpada de infravermelhos como fonte de calor. Foram testadas três configurações de distância entre as placas e dois tipos de lâmpadas para comparação. Este teste simularia, por exemplo, a transmissão de calor entre diferentes componentes dentro do satélite. Relativamente à condução, a maioria dos nano e microssatélites são compostos de *PCBs* empilhadas, mantidas juntas por espaçadores e varões roscados, conectados à estrutura principal. Esta é a principal forma de conduzir calor dos componentes para as superfícies irradiadoras. Associada à interface entre a *PCB* e os espaçadores, existe uma resistência térmica que é um parâmetro desconhecido com grande impacto nas análises térmicas. Desta forma, foi realizado uma segunda experiência para estudar a resistência térmica de contacto (ou condutância) entre uma *PCB* e espaçadores.

Paralelamente, o software de elementos finitos (MSC Nastran) é usado para realizar um estudo numérico das mesmas experiências. Os resultados da distribuição de temperatura das soluções numéricas e experimentais foram então comparados e os resultados foram discutidos. Finalmente, com os resultados obtidos durante os testes foi realizada uma análise térmica em estado estacionário ao 3-AMADEUS *CubeSat*.

Palavras-chave

Análise térmica de *CubeSat*, Radiação térmica entre placas paralelas, condutância térmica entre contactos, resistência térmica em interfaces, validação do sistema de controlo térmico, contacto entre circuitos impressos e espaçadores

Abstract

There has been an increasing interest in CubeSat missions due to its small size, low cost and flexibility to accommodate different payloads. New missions with highly temperature sensitive payloads, increased power dissipation (by continuous miniaturization of electronic components and systems) and reduced radiating surfaces lead the thermal loads issues into a bigger challenge. One of the causes of failure in a satellite in space is the temperature peaks suffered during a full orbital cycle. Therefore, proper thermal control system design and test should be performed to guarantee the reliability of a spacecraft prior to launch.

3-AMADEUS is a unity CubeSat currently being developed in a partnership between CEiiA and UBI. The purpose of this mission is to demonstrate that a attitude determiner and control system exclusively magnetic is able to provide a three axis orbital attitude for the nanosatellites. The present work aims to perform thermal analysis to 3-AMADEUS CubeSat in order to ensure its survival as soon as it is placed in orbit. Therefore, it is required the understand the main heat transfer processes within a satellite, conduction and radiation, in order to validate the current methodologies used for thermal analysis. Hence, with the purpose of developing thermal models with higher reliability, two experiments were devised to be performed in a vacuum environment.

The first experimental test consists in a study of heat exchange between two aluminum plates through radiation, using an infrared lamp as a heat source. Three distance configurations between plates and two lamp types were tested to comparison. This would emulate, for example, the heat transmission between different components within the satellite. Regarding the conduction experiment, most nano and micro satellites are composed of stacked PCBs, held together by spacers and rods and linked to the main structure. This is the primary mean to conduct the heat from the different components to the external radiating surfaces. A high thermal resistance is associated with the interface between the PCB and the spacers, which is an unknown parameter with a high impact on the thermal analysis. Therefore, a second experiment is carried out to study thermal contact resistance (or conductance) between them.

In parallel, finite element software (MSC Nastran) is used to carry out a numerical study of the same experiments. The temperature distribution results of both numerical and experimental solutions were then compared, and the results were discussed. It was concluded that the results obtained in both experiments, in general, presented a good agreement. Finally, with the results obtained in the numerical simulations and using the validated methodology, a steady state thermal analysis was performed to 3-AMADEUS.

Keywords

CubeSat Thermal Analysis, Thermal radiation between parallel plates, Thermal contact conductance, Thermal contact resistance, Thermal control system validation, interface between PCB and brass spacer

Contents

List of Figures

List of Tables

Acronyms List

AU	Astronomical Unit
CAD	Computer Aided Design
CEiiA	Centre of Engineering and Product Development COTS Commercial-off-the-shelf
ECSS	European Cooperation for Space Standardization
ESA	European Space Agency
FEM	Finite Element Analysis
GEO	Geostationary Earth Orbit
GPS	Global Position System
HEO	Highly Elliptical Orbit
IR	Infrared
ISIS	Innovative Solutions in Space
ISS	International Space Agency
LEO	Low Earth Orbit
LWR	Long Wave Radiation
MEO	Medium height Earth Orbit
MLI	Multi Layer Insulation
NASTRAN	Nasa STRuctural Analysis
OBC	On Board Computer
PCB	Printed Circuit Boards
PDE	Partial Differential Equations
RMS	Root Mean Square
TC	Thermocouple
TCS	Thermal Control System
TMM	Thermal Mathematical Model
TVC	Thermal Vacuum Cycling
UBI	University of Beira Interior

Nomenclature

$\delta 0$	Gap thickness parameter
δU	Internal Energy
$\dot{Q}_P lanet$	Emitted heat by Earth
$\dot{Q}_{Albedo}$	Reflected solar abortion energy
$\dot{Q}_{Sun}$	Solar radiation absorbed
A	Flat surface area
A_a, A_r	apparent and real contact areas
D	Distance between plates
E	Modulus Elasticity
E_b	Emissive power
F	Force
F_{ij}	View factor between surface i and j
F_{SC-P}	View factor between the spacecraft and the planet
G	Irradiation
G_s	Solar Constant
H	Microhardness
h_c	Contact Conductance
J	Radiosity
k	Thermal Conductivity
k_s	Effective thermal conductivity
L	Lenght
m_s	Effective absolute mean asperity slope
P	Pressure
Q	Rate of heat transfer
Q	heat flow rate
$Q_e xternal$	Environmental heat absorbed
$Q_i nternal$	Power dissipated by internal components
Q_{in}	Heat generated plus incident heat loads

Q_{out} Heat rejected

$Q_{radiated}$ Heat emitted to space

r Specimen radius

R_j Thermal contact Resistance

T Temperature

T_m Interface temperature

W Work done by the system

Greek Letters

α Absorptivity

ϕ Zenith Angle

ρ Reflectivity

σ Stefan-Boltzmann Constant

τ Transmissivity

ε Emissivity

Subscripts

$1,\ 2$ specimens 1 and 2

$i,\ j$ specimens i and j

Chapter 1

Introduction

This chapter is devoted to the presentation of the motivation to develop accurate thermal analysis to satellites. The context in which this thesis is developed, is introduced as well as the 3-AMADEUS project. The purpose of solving the problem and the contributions to the scientific community to overcome the upcoming thermal problems associated to CubeSats are presented. The objectives of this work are introduced and finally the thesis structure is explained.

1.1 Motivation

Since the first satellite was put in orbit over 50 years ago, satellites have increased in size and weight and consequentially the cost to launch them into space increased as well [1]. However, small satellites more properly CubeSats, have gained a particular interest and are revolutionizing the future of spaceflight. Their small size and defined standards allow it to be a multi-purpose and low cost platform, flexible to accommodate different payloads and the ability to perform several missions.

However, once in orbit, these temperature sensitive components can suffer fatal failure. The satellite is exposed to intense periods of solar radiation and umbra during the orbital cycles. This results in critical temperature peaks which could be the cause of failure of the full system [2]. Furthermore, the heat produced inside the satellite by electronics must be conducted to the external faces to be rejected through radiation to the surrounding environment. Therefore, all components inside the satellite must be operated in a certain operational temperature range. In order to do so, a thermal control system design, analysis and testing is critical on satellite's the development. The thermal analysis provide temperature distribution estimations which are used to guarantee that the thermal requirements are fulfilled and thus, confirming the reliability of the spacecraft prior to launch. Despite that, these analyses must be reliable and to make them so, is necessary to validate it through experimental tests.

It is necessary to understand how radiation is exchanged between surfaces in a vacuum environment, considering the entire enclosure. Radiation exchange between surfaces is highly influenced by surface characteristics and geometry, orientation and separation distance, known as view factors. Numerical calculation of view factors is a key point for thermal radiation problems since the calculations can be very complex. On one hand software is fully capable of performing these calculations, however error can be introduced derived approximations made. On the other hand, detailed analysis could be quite time consuming and a trade off must be searched.

Another important parameter usually unknown is the high thermal contact resistance is associated to the contact between spacers and PCB's. The heat flow path is important to control electronics temperature. Breaking this heat flow path could be dangerous and lead to overheat-

ing which could cause failure [3]. In past analysis a non measured value was used, rather it was used safety value, which gave temperatures different to those experienced in orbit. Therefore, estimating the thermal contact resistance between spacers and PCBs is a major challenge in thermal analysis of CubeSats.

Thermal contact conductance is influenced by several parameters and has been studied since 1960's. Numerous expressions and correlations were made in a vacuum environment. However, almost all of these studies involved two generic mating solids with a known-constant pressure. As a result of the uncertainty of pressure and lack of description of the process, determining the thermal contact conductance becomes difficult. Therefore, it is essential to perform specific experiments to gain knowledge about the actual value in a specific contact such as the spacer-PCB interface.

1.2 Purpose and Contribution

In the early years of CubeSats, thermal analysis were rarely done and when performed, low fidelity models were used with unknown parameters and material properties. Additionally, experimental test and flight data correlation with thermal models was not done, preventing CubeSat developers from improving their modeling. Therefore, accurate and validated analysis must be performed to the thermal control system of satellites prior to launch to assess it. In the light of this matter, it is proposed test rigs construction for experimental radiation and thermal contact conductance studies. It is expected that the findings validate and improve the accuracy of thermal analysis for better prediction the spacecraft and subsystems temperatures. Thus, minimizing the risk of failure and loss of the spacecraft once in orbit.

To accomplish the main purpose, it is essential to fully understand the heat transfer methods, in particular thermal radiation and conduction between two contacting bodies. These mechanisms are studied analytically and numerically. Subsequently, the results obtained are used to validate the actual thermal control system of 3-AMADEUS, currently being developed at CEiiA and UBI.

Additionally, CEiiA is participating in several space related projects, the work presented in this thesis presents a important contribution for actual and future thermal analysis. Currently, CEiiA uses MSC Nastran to perform thermal analysis. Therefore, numeric methods must be understood and validated through experimental data. Considering the work presented, CEiiA will be able to use the knowledge acquired for current and future projects thermal analysis, such as small satellites or even a launcher for further analysis.

1.3 Context

The goal of this thesis is to gain confidence when performing thermal analysis to satellites. Thus, the ultimate work intents to validate the thermal control of the 3-AMADEUS CubeSat. Since repairs can be done in space, after the satellite's launch, is crucial to validate t thermal control system. Thereby, it is assured that all the money invested in developing the satellite isn't wasted in case of thermal failure. Therefore, reliable thermal analysis and methodologies

must be pursued.

1.3.1 3-AMADEUS CubeSat Project

The 3-AMADEUS(3 Axis Magnetic Attitude Demonstration Experiment for a Unit Spacecraft) is a 1U CubeSat currently under development in a collaboration by CEiiA and UBI. At this point, magnetic attitude determination and control devices are one of the cheapest, most reliable, small and lightweight attitude systems. However, they have limitations, in particular a relatively low accuracy (2º to 10º depending on disturbing torques acting on the satellite) and actuation capability requiring attitude sensors and actuators. Therefore, the mission objective is to demonstrate that a solely magnetic Attitude Determination and Control System might e capable of providing three-axis orbital attitude for Nanosatellites. The attitude information gathered during the whole orbit is sent and send it to earth at appropriate times.

The spacecraft's orbit will be a 550 km approximately circular sun synchronous orbit. It will have the following orbit parameters:

Table 1.1: Orbital details of 3-AMADEUS's initial orbit

Epoch	1 Jan 2020
Orbit Type	LEO
Altitude of Apogee / Perigee	550km
Eccentricity	0
Inclination	97.58º
Argument of Perigee	0º
RAAN	270º
True Anomaly	0º
Orbital Period	96 min

1.4 Research and Objectives

The main goal of this thesis is to gain confidence and understand the main heat transfer processes that occur in a satellite in order to perform accurate thermal analysis. The following objectives were defined for this research are summarized as follows:

- Review the main technologies used for thermal control of CubeSats;
- Gather the currently methodologies, both numerical and experimental, used to validate the thermal control system;
- Develop test rigs to investigate two important heat transfer processes that occur in a satellite, emulate the same experiments thereby validating the thermal analysis;
- Estimate the thermal contact conductance between spacers and PCBs through an indirect method;
- Analyze and validate the current thermal control system of 3-AMADEUS and provide suggestions if necessary;

- Create a methodology to perform thermal analysis in points which are difficult to calculate, such as contacts.

The objective of performing the experiments leads directly to the thermal analysis of the 3-AMADEUS CubeSat and validation of the thermal control system. The validated numerical analysis will answer the question if whether or not the actual thermal control system is sufficient to survive the space thermal environment and provide insights where changes are needed.

1.5 Thesis Outline

This thesis is divided in seven chapters. The description of each chapter is mapped as follows:

Chapter 1 introduces the motivation to solve the research problem. It presents the purpose of this work and the contribution to the scientific community. Lastly, the objectives expected to be achieved during this study are presented.

Chapter 2 starts with an introduction to the satellites history. The CubeSat concept and the 3-AMADEUS project are introduced. The spacecraft subsystems division is presented, which allow to introduce the thermal control system and continues with a description of the space environment.

Chapter 3 presents the theoretical basics of heat conduction and thermal radiation necessary to define the heat balance equations for the thermal modeling of satellites. The main theories for thermal contact conductance estimation are presented. Finally, numeric heat transfer methods, the basics of FEM and the Software are introduced in this Chapter.

Chapter 4 describes both experimental tests performed and test rig development. Data acquisition system assembly and test facility are described in this chapter. Material, schematics and procedure are explained in this chapter. The experimental results are presented and discussed.

Chapter 5 details the numeric analysis of the experimental tests performed. The modeling steps and boundary conditions attributed are presented. Finally, the numerical results for both analysis are presented, compared with experimental data and discussed.

Chapter 6 characterizes 3-AMADEUS CubeSat and provides the steps taken to develop the thermal model. The simulation cases, worst case scenarios, are formulated and described. Thermal analysis results are presented and conclusions made.

Chapter 7 recaps the work performed with a conclusion and achievements obtained. Difficulties suffered performing the experiments are presented. Solutions to solve these difficulties are discussed.Finally open points and future work recommendations are provided.

Chapter 2

Literature Review

This chapter details the important role satellites play, being practically indispensable in all humanity activities such as scientific, telecommunications and Earth observation missions. The CubeSat concept is introduced, as well as the spacecraft subsystems division. Satellites have to survive extreme conditions. This allows to introduce the expected space environment, focusing on heat sources of a satellite in Earth's orbit. Theory for environmental heat inputs calculation is presented. Finally, thermal control system and main thermal control technologies are presented.

2.1 Satellite History Overview

Satellites can be split into natural and artificial and they can orbit either a planet or the sun. The moon is a good example of a natural satellite because it orbits Earth. Nowadays, artificial, or man-made machines launched to space are referred simply as "satellites". These machines are used primarily for communications, monitoring the weather and climate changes, for security, for beaming television signal, for secure, robust three dimensional position (navigation) and technology demonstration. Nowadays, as we can't live without computers, cars or mobile phones, we are fully dependent of satellites [4, 5].

The story of artificial satellites begins well before the first launch of a satellite. Isaac Newton was the first to imagine how a man-made satellite could orbit Earth in is *Principia mathematica* (1687). He theorized a cannon firing a ball from the top of a very high mountain that if fired with sufficient power would 'describe the same curve over and over'. However, he didn't think of a satellite as a concept as we know today or it's usefulness. At that time, there wasn't a rocket powerful enough to put a satellite in orbit. Tsiolkovsky, in 1903, showed how satellites could be launched and calculated the required velocity in order to put a satellite into orbit. By the early twentieth century, the World Wars led to a period of high technological development, which started a race between the US and the Soviet Union to be seen which one would launch the first satellite. The Soviets won by launching Sputnik I in 1957, leading to the begging of Space Age. Since then, almost 8500 satellites were launched by more than 40 countries [6, 7].

Considering Portugal, PoSAT-1 was the first and only Portuguese satellite launched to space in 1993. It weights around 50kg and was used to test technology for future missions [8]. In 2020 is scheduled to launch Infante, the first developed and built satellite in Portugal. This will be a satellite mainly focused on maritime applications and will be developed by a consortium in which UBI and CEiiA are included. Furthermore, last year, Manuel Heitor, Portugal's science and technology minister announced that fourteen enterprises were interested in building a space station in Azores. It's expected that the first launches will take place in 2021. The main focus will be launching small satellites. Thus, if successful, this program will be a major step for

Portugal space industry, because it will attract companies dedicated to satellite development and therefore creating more workplaces [9].

Satellites can be classified by size, orbit, type of payload and therefore mission objective. They can vary from the size of a pickup truck to just the size of a small shoe box and have all shapes. Small satellites are defined as satellites weighing less than 500 kg. However, with the arrival of CubeSats and other very small satellites, it was necessary to create more terminology. The common classification by weigh is listed in Table 2.1.

Table 2.1: Satellite classification in terms of deployed mass and cost [10, 5].

	Category	Mass range (kg)	Cost(M€)
	Large satellite	>1000	>116
	Medium-sized satellite	500 - 1000	29-116
Small Satellites	Minisatellite	100 - 500	8-29
Small Satellites	Microsatellite	10 - 100	1-8
Small Satellites	Nanosatellite	1 - 10	0.1-1
Small Satellites	Picosatellite	0.1 - 1	<0.1
Small Satellites	Femtosatellite	<0.1	<0.1

Besides the different size,satellites can be divided accordingly to their mission. The main type of missions include interplanetary spaceflight, military and intelligence, commercial, science and applications, technology demonstration and education. Table 2.2 presents some payload/mission types as well as commonly used orbits and examples of missions.

Table 2.2: Space mission applications, common used orbits and examples [1].

Mission	Trajectory type	Examples
Communications	Geostationary for low latitudes, Molniya and Tundra for high latitudes (mainly Russia), Constellations of polar LEO satellites for global coverage	IntelSat Iridium
Earth resources	Polar LEO for global coverage	SPOT SeaSat
Weather	Polar LEO, or geostationary	TRMM NOAA
Navigation	Inclined MEO for global coverage	GPS GLONASS Galileo (ESA)
Astronomy	LEO, HEO, GEO and 'orbits' around Lagrange points	Hubble JWST
Space environment	Various, including HEO	Polar SORCE
Military	Polar LEO for global coverage, but various	DSP MILSTAR
Technology demonstration	Various	CubeSats

Note: GEO: Geostationary Earth Orbit; HEO: Highly elliptical orbit; LEO: Low Earth Orbit; MEO: Medium height Earth Orbit.

The first satellite placed into orbit over 62 years ago was considered a "small" satellite. Although the size and complexity of satellites have grown considerably since that time, ironically the space industry is returning and evolving to smaller satellites. CubeSats, in particular, have gained a unique interest by students interested in space science, technology and missions. Companies are also attracted by the CubeSat market, searching for more affordable alternatives [11].

2.2 Spacecraft Subsystems

Satellites system are divided in several subsystems as can be seen in Figure 2.1. This division reduces the interaction between subsystems and improve coordination between the different subsystem engineers [1]. This subsystems must provide the spacecraft ability to complete its mission. Therefore, the spacecraft must be able for example to point the payload in the right direction, change or correct the orbit, allow communications with the ground and energy management [5].

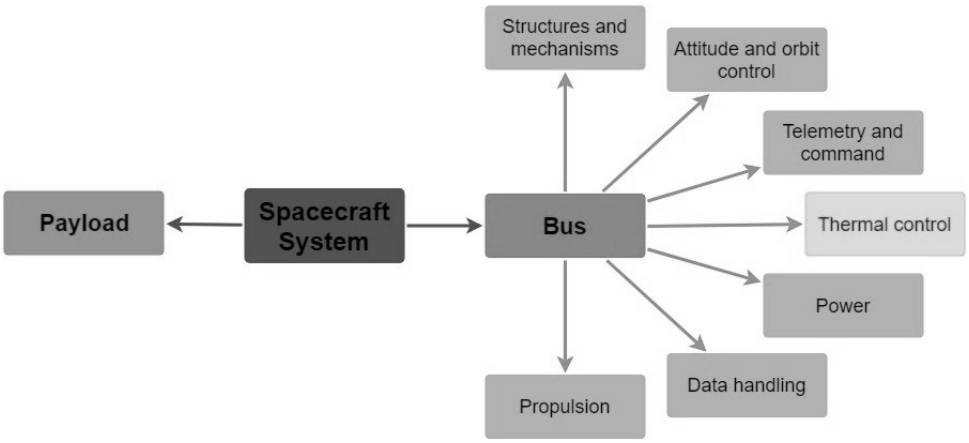

Figure 2.1: Satellite subsystems division [1].

Although they are not directly connected between them, the design of each system or subsystem has direct impact and resources implication on the others [5]. Of all the subsystems the main focus of this thesis will be the thermal control system.

2.3 CubeSats

The term ”CubeSat” refers to a cube-shaped satellite measuring 100 mm × 100 mm × 100 mm and having a mass no greater than 1.33 kg. Prof. Jordi Puig-Suari at California Polytechnic State University and Prof. Bob Twiggs at Stanford University’s Space Systems Development Laboratory conceived the CubeSat standard in 1999 [12]. The original purpose of the project was to provide affordable access to space for the university scientific community. The main idea was that a ”learn-by-doing” approach would provide students with hands-on experience in the field of spacecraft design and development [13]. However, in recent years a growing number of CubeSat missions indicate that the first CubeSats were almost as starting point for educational and technology demonstration. Thus, becoming a low-cost platform that could have science data return with high value and commercial revenue [14].

The specific standards for CubeSats help reduce the costs of technical developments and scientific investigations. These standardized aspects of CubeSats enable companies to mass-produce components and offer commercial-off-the-shelf parts (COTS). Therefore, the engineering and development of CubeSats becomes less costly than small satellites with customized design. Also, the costs associated to transporting and deploying them into space are reduced because of the standardized shape and size, and the possibility to launch several CubeSats with a single rocket

launch [15].

The standard size of a CubeSat is referred to 1U, with U representing a ”unit”. However, CubeSats can be aggregated to form a variety of sizes, such as the 1.5U, 2U, 3U and 6U [15]. Larger configurations are always in development as can be seen in Figure 2.2.

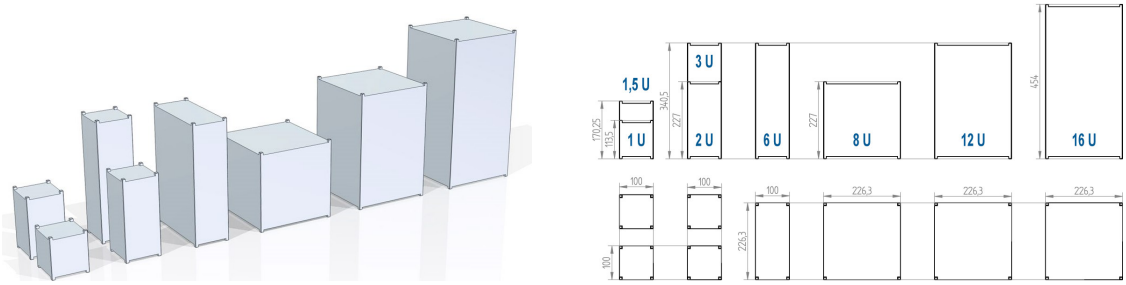

Figure 2.2: CubeSats sizes from 1U to 16U [16].

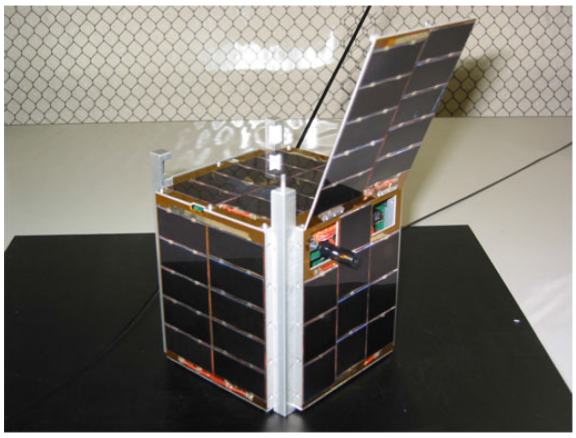

Figure 2.3: CUTE-I satellite flight model [17].

One of the first CubeSats launch to space was the CUbical Titech Engineering (CUTE-I) satellite (Figure 2.3), developed by the laboratory for Space Systems at the Tokyo Institute of Technology and launched on June 30, 2003. CUTE-I had three objectives: 1) demonstrate the ability to successfully download various satellite telemetry data in order to know the satellite conditions, 2) use the downloaded sensor data to calculate the satellite’s three-axis attitude and 3) demonstrate the effectiveness of a small deployment mechanism [17]. As can be seen in Figure 2.4, more than 1000 CubeSats were launched by 61 countries until this point and for the next 6 years over 3000 nanosats are expected to be launched [18].

The next years will show the evolution of the CubeSats applications. One example is the networks of small satellites which distribute the tasks of a single common satellite. This network ideally would be autonomous, flexible, dynamically re-configurable, redundant and readily deployable [11].

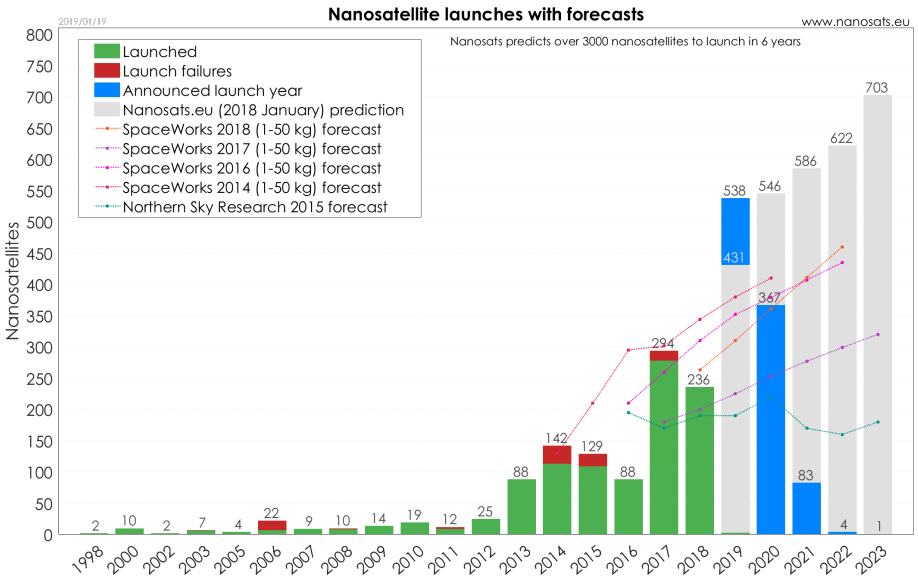

Figure 2.4: Nanosatellite launches with forecasts for the next years [18].

2.4 Space Thermal Environment

Given the mission orbit parameters, the first step in any thermal analysis starts with the identification of the sources of heat incident upon a satellite. The environment of a spacecraft is of extreme importance for the thermal management system. The main sources of environmental heating are direct solar radiation, Earth Albedo and Earth IR. These radiation fluxes depend on the orbital parameters, size, shape, view factors and surface properties of the spacecraft [19]. Furthermore, space can be considered as a heat sink at 3 K [20]. Figure 2.5 illustrates the main heat sources in space.

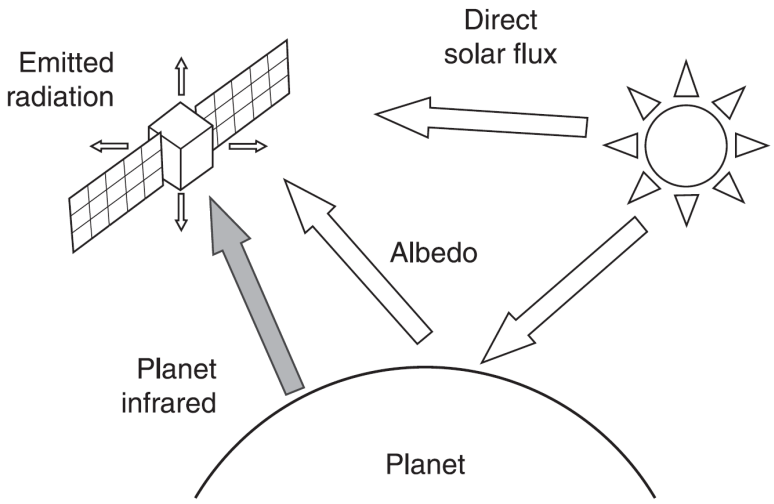

Figure 2.5: Satellite thermal environment in Earth's orbit [21].

2.4.1 Direct Solar Radiation

Sunlight is the main heat power source of a spacecraft in Earths orbit. For thermal purposes,

the sun's spectral distribution can be approximated as a blackbody at $5762\ K$ [20] emitting primarily shortwave radiation. The value of the solar constant, the intensity of incident energy at 1 AU (Earth's mean distance from the sun), is equal to $G_S = 1366.1 W/m^2$. However, this value isn't constant due to the the 11 year solar cycle and the Earth's orbit. The first case has very little effect on the radiation emitted from the sun. The second case causes a variation of about 3.4% as a result of the eccentricity of the elliptical orbit which produces a geometrical variation in the distance between the Earth and the Sun. Therefore, the electromagnetic radiation values range from a minimum of $1321.6\ W/m^2$ at aphelion (summer solstice) and a maximum of $1412.9\ W/m^2$ at perihelion (winter solstice) [19, 21, 20].

With a simple equation is possible to calculate the solar radiation absorptivity by a flat surface of area A, whose normal vector forms an angle θ with the solar rays:

$$\dot{Q}_{Sun} = \alpha G_S A cos\theta \tag{2.1}$$

where α is the material solar absorptance of the surface and dependents on the surface's finish [21].

2.4.2 Earth Albedo

The albedo of the Earth is the portion of the total incident solar radiation reflected by the planet to space. Its influence for thermal design is higher for low orbits. The value of Earth albedo vary with location and time. The main influences are the Earth's topography and meteorological conditions. Other factors are the solar elevation angle and the spectral content of incident solar energy. As a result of the planet's surface roughness albedo is assumed to be diffuse.

Generally, reflectivity increases with a increasing cloud coverage and a decreasing solar elevation angle, which varies during a day and seasonally. Additionally, varies with the Earth's surface, being greater over continental regions than oceanic regions. In continental areas the albedo decreases with moisture. It can vary from small values over forests and higher values over desert areas. As for the ocean areas, since they absorb most of the incident radiation the albedo is between 0.05 and 0.1. Because of the high snow and ice coverage close the poles, associated with increasing cloud coverage and a decreasing solar elevation angle, albedo tend to increase with latitude [22]. The mean albedo value for Earth is assumed as 0.3, however, it must be used with care. A model to estimate the influence of latitude and longitude on albedo have been developed by the European Space Agency in [20].

When calculating the thermal loads on a satellite, it must taken in consideration that albedo loads must be used only when the portion of the planet seen by the spacecraft is sunlit. For simplified calculations, assuming the planet behaves as a reflecting sphere, the energy absorbed from albedo loads by an area A is

$$\dot{Q}_{Alb} = a G_S A F_{SC-P} cos\phi, for -\frac{\pi}{2} \leq \phi \leq \frac{\pi}{2} \tag{2.2}$$

where a is the planet albedo, F_{SC-P} the view factor between the spacecraft surface and the

planet and ϕ the zenith angle.

2.4.3 Earth Infrared Radiation

A fraction of incident sunlight is absorbed by the Earth and its atmospheric gases. The Earth IR, or long wave radiation (LWR), is the emitted thermal radiation and it's constant annually. Nevertheless, the intensity varies with time and from location to location on Earth's surface. It depends on the local surface temperature and the cloud coverage. Warmer surface areas, such as deserts and tropical regions, will emit more radiation than colder areas. Cloud coverage will decrease the LWR, since lower clouds absorb radiation coming from the surface and the clouds top are at colder temperatures. In the case there are no clouds, the atmospheric temperature and moisture content become the main factors. The Earth IR unlike albedo has less variation across the globe [22].

The average temperature of the Earth's surface is about $255\ K$ and the emitted thermal radiation has a spectrum of a black body. This corresponds to an average flux of $230\ W/m^2$. This value can range from $150\ W/m^2$ to $350\ W/m^2$ for an orbiting spacecraft. Over ocean areas this flux is more constant during the day than over desert areas [20]. With the planet's average temperature, the flux incident on a spacecraft surface of area A can be obtained from:

$$\dot{Q}_{Planet} = \epsilon A F_{SC-P} \sigma T_P^4 \tag{2.3}$$

where ϵ is the infrared emissivity of the satellite surface and T_P the temperature of the planet [21].

Earth albedo loads and infrared radiation are important for low orbits. However, for weather satellites in geostationary orbits these loads are insignificant, because of the low view factor. In Table 2.3 it is summarized the heat sources explained above.

Table 2.3: Summary of Heat Sources

Heat Source	Value
Direct Solar Radiation	$1367\ W/m^2$
Earth Albedo	$0.3 * 1367\ W/m^2$
Earth IR	$230\ W/m^2$

2.5 Thermal Control System

The thermal control system must maintain a temperature stability using the less system resources possible. These limit temperatures are pre-defined upon the critical internal components. Examples of typical temperature requirements for main spacecraft components are -20 to +50 to electronic equipment and 0 to +20 for batteries. Controlling the components temperature not only ensures the reliability of the spacecraft, but also guarantees the optimum performance, preventing early degradation and success of the mission [5].

The hardware to control the temperature inside the satellite can be either active and/or passive. Each one is described in the following sections and examples are given.

2.5.1 Passive Thermal Control Systems

A passive thermal control technique is characterized by do not requiring input power nor moving parts for thermal regulation and are associated to low cost, volume, weigh and risk. Also, are proved to be reliable. They are the primarily technique for thermal control, relying on thermal conduction, radiation exchange and insulation systems [23]. Several options are readily available to CubeSats. Some examples are summarized bellow.

Coatings and surface treatments are used to change optical properties of a surface. Thus, the thermal radiation environment is manipulated. The solar absortance and IR emittance can be varied according to the purpose needed and must be selected in order to achieve an energy balance at a desired temperature [19]. In small satellites the use of thermal tapes is easy to either apply or remove, and last longer than paints [24, 25].

Multi-layer insulation (MLI) or single-layer radiation barriers are used to insulate a satellite from radiation coming from the sun and reduces energy dissipation. MLI are composed of multiple layers of highly reflecting shields separated by non-metallic and low conductivity spacers in order to prevent contact between layers [19]. The use of MLI outside small satellites is uncommon due to the low efficiency in small areas, the outside surface being covered by solar cells and the necessity of rails clearance, due to the use of a deployer.

Thermal straps work with the same purpose of the heat pipes: transport thermal energy, passively, from heat generator components to a thermal sink. They are usually manufactured in aluminum or copper, however recently efforts were put in developing more flexible thermal links using pyrolitic graphite and graphene sheets [23].

2.5.2 Active Thermal Control Systems

When CubeSats have high power demand, passive systems could be insufficient. Also, active systems are suited to applications where the spacecraft suffers large thermal fluctuations or seasonal variations, requiring thermal control for specialized payloads [23, 5]. However, the reduced size of CubeSats, limits available options of active thermal control systems. It's witnessed that the major quantity of active systems used in CubeSats consist in conventional technology used in larger satellites, which is size reduced in order to adapt to the small size of CubeSats.

Heaters consist in a electrical-resistance element between two layers of flexible electrically insulator material. Due to its flexibility they can be simply attached to any surface. The main disadvantage of heaters is the high energy consumption [19, 25].

Some payloads, such as high precision infrared sensors, imaging spectrometers, interferometers, require extremely low temperatures to operate. Temperatures less than 50K can be achieved through the use of cryocoolers [26].

2.6 Thermal Verification Tests

Thermal verification tests must be performed in order to validate the thermal model. The main objectives of thermal testing are: looking out for environmental stress, turn-on capabilities, survival demonstration, ETC [19]. The tests can be divided in two categories. One that confirm the validity of thermal control and other that endorse component's integrity and workmanship [27]. These tests must be performed under a pressure of $\leqslant 10^{-5} hPa$ or less accordingly to ESA standards [28]

The validation of the thermal control system prior to launch is done through a thermal balance test. This test must be performed in controlled environment in specialized laboratories as can be . The need for this test is determined on a per project basis [29]. The objectives of performing this test, as defined by the European Cooperation for Space Standardization (ECSS), are to provide data for verification of the numerical model in order to qualify the TCS, to demonstrate the appropriateness of the TCS design verify the performance of the TCS hardware, either active and/or passive, and to provide sensitivity data regarding certain components of the thermal control system [20].

ESA standards recommend performing two different steady-state cases and a transient case for components subjected to dynamic thermal behavior to validate the worst case scenarios [20].

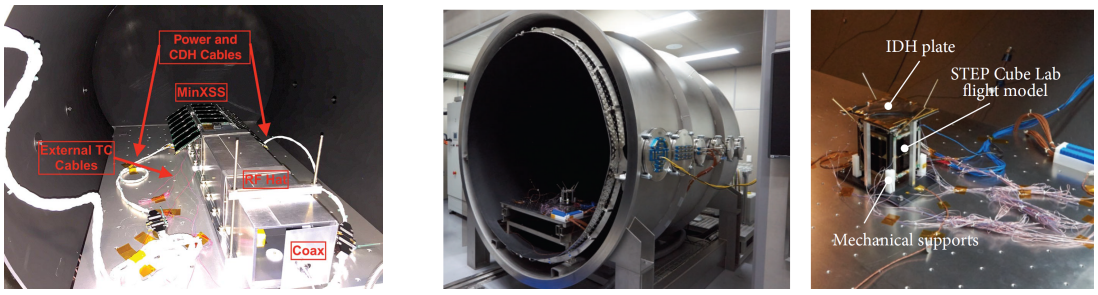

(a) MinXSS-1 in Bemco-West themal vacuum chamber [25]

(b) Thermal vacuum test set-up of STEP Cube Lab [30]

Figure 2.6: CubeSat's thermal vacuum testing.

When the temperatures reached during the thermal balance test, are close enough to the predicted in the thermal model, the test is considered successful. Typical values for temperature deviations are defined by the ECSS. As can be seen in Table 2.4, the temperature deviation for internal and external components must be lower than 5 and 10K respectively. For the temperature mean deviation a minimum of 25 measurements correlation is needed [20].

Table 2.4: ECSS defined correlation success criteria [31].

Temperature deviation for internal temperatures	$< 5K$
Temperature deviation for external temperatures	$< 10K$
Temperature mean deviation	$\pm 2K$
Temperature standard deviation	$< 3K, 1\sigma$

A philosophy of safety margins applied to the calculated temperature ranges, in order to define qualification and acceptance tests, according to ESA Standards [20]. These margins are illustrated in Figure 2.7.

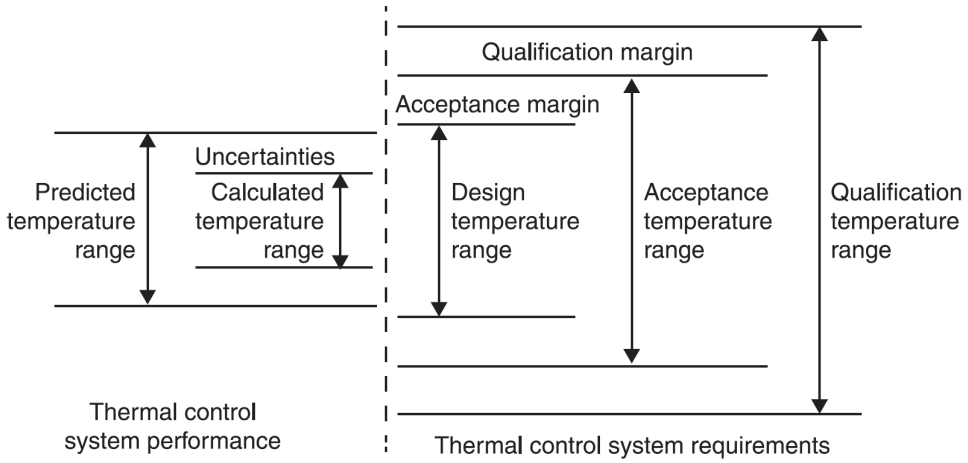

Figure 2.7: Temperature definitions for thermal control system [31].

CubeSat developers do not need to perform the thermal vacuum cycling test (TVC) mandatorily. In this test, the spacecraft is exposed to a certain number of cycles, with pre-defined holding times and with given minimum and maximum temperatures. This test serves to check if there are any problems related to thermal stresses associated to temperature variation cycles on orbit, by revealing any issues regarding malfunctioning or flawed components [15, 19].

Besides testing, a thermal vacuum bakeout is a requirement made by the launch providers to secure other missions in the same launcher. This is made to ensure proper outgassing of any possible contaminants of components before the actual launch [12]. Furthermore, it makes sure that optical and sensitive payloads aren't contaminated. [15].

Chapter 3

Heat Transfer and Thermal Analysis in CubeSats

In this chapter, the basics of heat conduction and thermal radiation are explained. Its understanding is vital to define the heat balance equations for the thermal modeling of satellites. Numeric heat transfer methods and the basics of FEM are introduced. A survey of the current methodologies used for CubeSat thermal analysis is performed. The theory presented will be necessary in the Chapters ahead.

3.1 Heat Transfer

Heat transfer is the science that deals with prediction of the rates at energy is transferred from one system to another because of a temperature difference. On the other hand, thermodynamics deals with equilibrium states and energy balance of all type of systems [27, 32]. For the thermal analysis of a spacecraft, the First Law of Thermodynamics states that energy can't be created or destroyed, only transferred:

$$\Delta U = Q - W \tag{3.1}$$

which simply states that the the rate of heat transfer to a system, Q, minus the amount of work done by the system, W, equals the variation of the internal energy, ΔU, of a closed system.

The global thermal control of a spacecraft is achieved by balancing the heat rejected by the body against all the incident heat loads and the internal heat generated by the electronic subsystems (some of the power used by the electronics is released in the form of heat loads). From a generalized heat balance equation for conservation of energy:

$$Q_{out} = Q_{in} \tag{3.2}$$

$$Q_{Radiated} = Q_{External} + Q_{Internal} \tag{3.3}$$

where $Q_{Radiated}$ is the heat emitted by the spacecraft to deep space, $Q_{External}$ is the environmental heat absorbed, and $Q_{Internal}$ is the power dissipation by the internal electronics.

There are three mechanisms of heat transfer: convection, conduction and radiation. The last two are the main phenomena of heat transfer within a spacecraft in orbit. Convection is not observed in space because all systems of the spacecraft are in a vacuum environment. However, occurs for the most part on the ground, during ascent and in heat transfer from fluids contained

inside the satellite [27].

3.1.1 Conduction

Conduction is the process of heat transfer from particle to particle within a material or from two or more contact bodies. This indicates that in order for conduction to occur, a temperature gradient must present across the body. The process is given by Fourier's Law :

$$q_x = -kA\frac{\partial T}{\partial x} \tag{3.4}$$

where q_x is the heat transfer rate, k is the thermal conductivity, A the cross sectional area perpendicular to the direction of heat transfer and $\frac{\partial T}{\partial x}$ is the temperature gradient in the direction of the heat flow. The negative sign indicates heat flow from higher to lower temperatures [32].

Thermal conductivity is a material property that in most cases depends on the temperature. However, this value is almost constant within the temperatures observed in satellites. For spacecraft, the material properties and geometry of a system have an important role in the dissipation of heat generated by the electronics.
The Fourier equation ca be related to the Ohm's law in electric-circuit theory as:

$$Heat\ flow = \frac{thermal\ potencial\ difference}{thermal\ resistance} \tag{3.5}$$

Thus, the electrical analogy can be used to solve complex problems, using both thermal resistances in parallel and in series.

3.1.1.1 Thermal Contact Conductance

When two materials are in physical contact with each other, illustrated in Figure 3.1a, heat is conducted from one face to the other and is subjected to a thermal contact resistance, defined as

$$R_j = \frac{\Delta T_j}{Q} = \frac{T_{2A} - T_{2B}}{qA_a} \tag{3.6}$$

where the thermal contact resistance is defined as the ratio between the temperature drop across the interface and the total heat flux over the interface. The thermal contact resistance causes a drop in temperature over the interface, as can be seen in Figure 3.1b [19].

The main reason for the contact resistance, is the fact that surfaces, which seem to be smooth, on a microscopic level reveal asperity. This causes a reduction in the real contact area between the two contacting surfaces. The real contact area is just a small fraction of the apparent area [33]. The fraction between the actual and apparent area, A_r/A_a, depends on several parameters such as the surface roughness and waviness, surface hardness and contact pressure. Figure 3.2 shows the microscopic view of an interface.

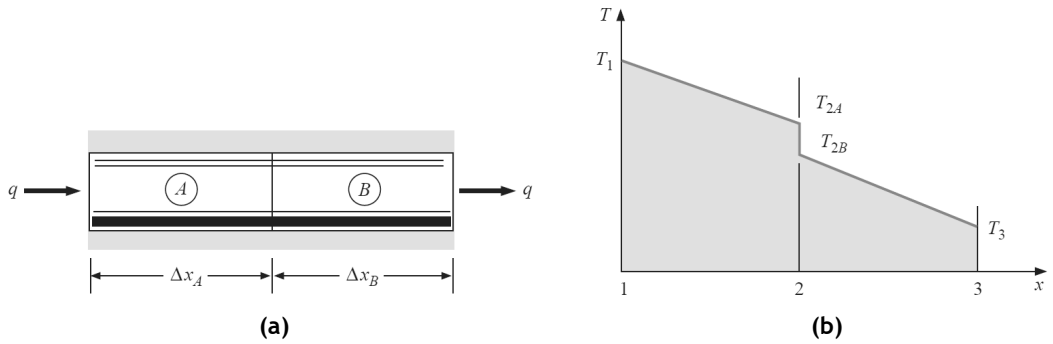

Figure 3.1: Thermal contact resistance: (a) interface between two materials ; (b) temperature profile of a contact [32].

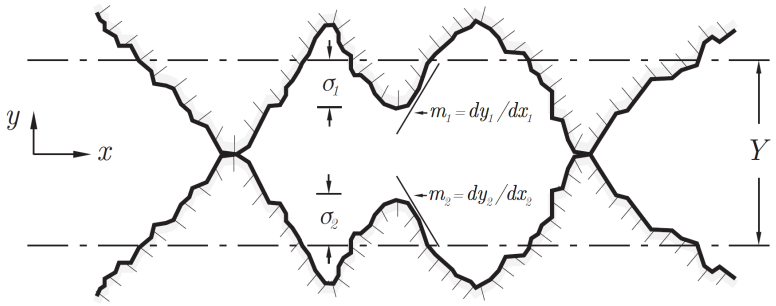

Figure 3.2: Representation of the heat flow through rough contacting surfaces, with emphasis to the microscopic phenomena [34].

Contact conductance, more commonly used in literature, is defined as the inverse of the resistance

$$h_j = \frac{1}{R_j A_a} \tag{3.7}$$

The heat transfer through the interface is considered to be the sum of three components. Contact conductance, h_c, the conduction through the actual contacting points. Gap conductance, h_g, conduction through the interstitial medium. Radiative conductance, h_r, thermal radiation between both surfaces. However, for bodies in space, which is a vacuum environment, the heat cannot be transferred through the medium. Furthermore, radiation can be neglected for most of space applications due to the low temperatures involved. Therefore, for the purpose of this thesis, the thermal joint conductance can be assumed to equal the contact conductance [19, 35].

Thermal contact conductance is affected by several factors, depending mainly on the two materials in contact. The main parameters are listed below [19, 35].

- The thermal conductivity of the contacting materials;
- The contact pressure;
- The surface roughness;
- The surface hardness;

- The average temperature of the junction.

The engineer must be cautious when choosing a model to use in satellite design calculations. Assumptions made for each model should be taken in account [19].

3.1.1.2 Related Work

Several studies were made to estimate thermal contact conductance in common CubeSat stacks. Berggren in 2015 performed experiments to measure the thermal conductance between a PCB and the mounting screw associated to a sleeve. The mean value obtained for the conductance was $G_{mean} = 0.0160\ W/K$ which correlated well with the theoretical calculated value [36]. Flecht in 2016, compared the results from simulations with measurements of an actual model. Finally, the contact conductance in the thermal model are adjusted to match the engineering model [37].

Recently, Hager [38] performed experiments with eight different configurations in vacuum. For aluminum spacers without washers the contact resistances was found to be ranging from 33.500 to $107.000\ W/m^2K$.

3.1.2 Radiation

Although heat transfer within a satellite can occur by radiation and conduction, the only means by which the vehicle can exchange heat with its environment is by radiation. Mechanisms to control temperature, either active or passive, must reject heat by radiation to space. Therefore, an accurate analysis of the radiant heat transfer is of extreme importance for better prediction of the spacecraft and subsystems temperatures.

All bodies emit and absorb electromagnetic energy when their temperature is above absolute zero. This process is known as thermal radiation, which is ruled by the amount of radiant energy emitted by a blackbody per unit time and per uni area E_b, also known as Stefan-Boltzman law, which states that total energy emitted is proportional to absolute temperature to the fourth power:

$$E_b = \sigma T^4 \tag{3.8}$$

where T is the body's temperature in Kelvin ans σ is the Stefan-Boltzmann constant, which has the value $\sigma = 5.669 \times 10^{-8}\,\mathrm{W/m^2 \cdot K^4}$. E_b is in watts per square meter and is named *emissive power* of a blackbody [32].

3.1.2.1 Radiation Properties

Equation 3.8 have been developed for a blackbody which is an idealized object that appear black to the eye and absorbs and emits all incident radiation. However, no object is a perfect black body, real bodies absorb, reflect and transmit incident, as shown in Figure 3.3. We define absorptivity, reflectivity and transmissivity as:

$$Absorptivity\ \alpha = \left(\frac{amount\ of\ absorbed\ radiation}{total\ incident\ radiation}\right),$$

$$Reflectivity\ \rho = \left(\frac{amount\ of\ reflected\ radiation}{total\ incident\ radiantion}\right),$$

$$Transmissivity\ \tau = \left(\frac{amount\ of\ transmitted\ radiation}{total\ incident\ radiation}\right),$$

Therefore, from the energy balance, the sum of these properties must be unity:

$$\alpha + \rho + \tau = 1 \tag{3.9}$$

Furthermore, for almost all solid objects that are opaque, no thermal radiation gets transmitted through, $\tau = 0$. Thus, $\alpha + \rho = 1$ [39].

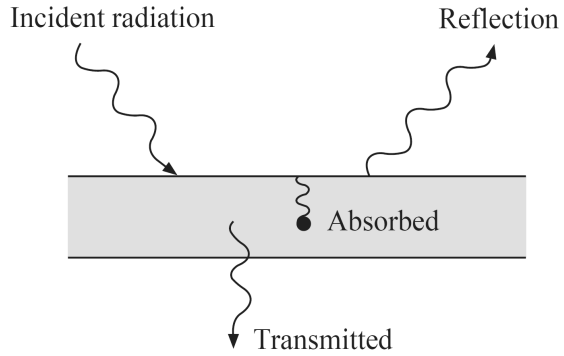

Figure 3.3: Absorption, reflection and transmission of a real body [32].

As stated before, real objects have lower emissivities than ideal black bodies. The emissivity is a function of the wavelength, the surface's temperature and surface roughness. However, for most of the engineering applications, emissivity assumes typical values shown in literature [32]. Figure A.1 in Appendix A shows surface characteristics of several materials, paints and coatings commonly used in satellites.

The spectral, hemispherical emittance, compare the real spectral emissive power with the spectral emissive power of a black body surface and is defined as

$$\epsilon_\lambda(T, \lambda) = \frac{E_\lambda(T, \lambda)}{E_{b\lambda}(T, \lambda)} \tag{3.10}$$

For a blackbody, the emissivity is $\epsilon = 1$ and for a real body $0 < \epsilon < 1$. So, the total emissive power of a real object becomes dependent on the emissivity:

$$E = \epsilon \sigma T^4 \tag{3.11}$$

3.1.2.2 View Factors

Above, thermal radiation on a single surface is discussed. However, in a space environment,

energy exchange between two surfaces must be considered and analyzed. The view factor, or shape factor, from a surface *m* to a surface *n* is denoted by $F_{m\to n}$ and is defined as the fraction of the radiation leaving surface *m* that strikes surface *n* [32]. The view factors only depend on the geometry, size, orientation and distance between the surfaces. Considering two differential areas as shown in Figure 3.4 it's possible to determine the differential view factor between them by:

$$dF_{dA_1\to dA_2} = \frac{cos\theta_1 cos\theta_2}{\pi r^2} dA_2 \tag{3.12}$$

where θ is the angle measured between a normal to the surface and the line that connects them r. Integrating over two areas, A_1 and A_2, the view factor between two diffuse finite areas is defined as:

$$F_{dA_1\to dA_2} = \frac{1}{A_1}\int_{A_2}\int_{A_1} \frac{cos\theta_1 cos\theta_2}{\pi r^2} dA_1 dA_2 \tag{3.13}$$

An important property of equation 3.13 is the reciprocity relation which is stated mathematically by:

$$A_i F_{ij} = A_j F_{ji} \tag{3.14}$$

Considering an enclosure, the general relation states that the sum of all view factors must be unity. For an enclosure with n surfaces the general relation is:

$$\sum_{j=1}^{n} F_{ij} = 1.0 \tag{3.15}$$

View factors can be calculated using analysis, numerical methods and analogy. The calculation presented is not practical, because even for simple geometries the integrations can be very difficult and complex. For the purpose of this thesis and for common geometries, such as that found in CubeSats, view factors are given in analytical, graphical and tabular form in several publications [40].

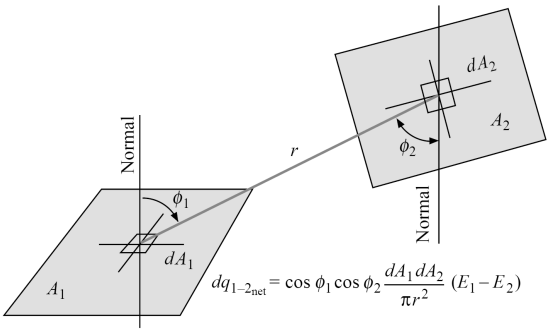

Figure 3.4: Radiative exchange between two area elements [32].

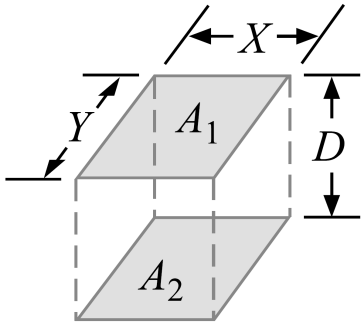

Figure 3.5: Radiation view factor for radiation between parallel plates [32].

3.1.2.3 Radiative Exchange Between Surfaces

For the purpose of this thesis, surfaces are assumed to be, diffuse and isothermal, in order to simplify the analysis and because nonblack bodies are involved [32]. Under these conditions and since transmissivity is assumed to be zero $\epsilon = \epsilon_\lambda = \alpha_\lambda = \alpha = 1 - \rho$. The total heat flux leaving a surface per unit time and per unit area is

$$J = \epsilon E_b + \rho G \tag{3.16}$$

where J is the radiosity and G is the irradiation, which is the total amount of energy incident upon a surface. By using the concept of gray and diffuse surface, radiosity becomes

$$J = \epsilon E_b + (1 - \epsilon) G \tag{3.17}$$

Solving for G in terms of J, the net energy leaving a surface is given by

$$q = \frac{J - G}{A} = \frac{E_b - J}{\frac{1 - \epsilon}{\epsilon A}} \tag{3.18}$$

where the numerator is considered as a potential difference, while the denominator is an opposition to heat transfer. This interpretation allows the radiation analysis by the network method originated by Oppenheim [41]. Considering the heat exchange between two surfaces, illustrated in Figure 3.4, the net interchange between the two surfaces is

$$q_{1-2} = J_1 A_1 F_{12} - J_2 A_2 F_{21} \tag{3.19}$$

Analytically the view factors for parallel plates (Figure 3.5) are given by:

$$F_{1-2} = \left(\frac{2}{\pi xy}\right) \left\{ \ln \left[\frac{1 + y^2}{1 + x^2 + y^2} \right]^{1/2} \right.$$
$$\left. + x \left(1 + y^2\right)^{1/2} \tan^{-1} \left[\frac{x}{(1 + y^2)^{1/2}} \right] + y \left(1 + x^2\right)^{1/2} \tan^{-} 1 \left[\frac{y}{(1 + x^2)^{1/2}} \right] - x \tan^{-1} x - y \tan^{-1} y \right\} \tag{3.20}$$

Other problems such as the three-body or the case of two surfaces enclosed can be solved by this method and are also important for this analysis [32].

3.2 Numeric Heat Transfer Methods

There are three methods to solve any engineering problem, the analytical, numerical and experimental methods [42].
Experimental investigation involves the construction of full-scale model, used to get actual temperature measurements. This method is expensive and slow, since it requires at least 3 to 5

measurements.

Analytical methods using the conservation of energy principle as differential equations attempt to predict temperatures, solving using initial and boundary conditions. This method is only applicable to simple cases of geometry, loading and boundary conditions.

Numerical methods attempt to predict/approximate the satellite's temperature. This method subdivides the satellite into nodes or elements that are connected by conduction and radiation. Therefore, a numerical solution enables the determination of temperature only at discrete points.

At an early stage of design of a satellite, experimental methods are extremely expensive and time consuming. Besides that, the number of different material properties and other nonuniformities would require immeasurable number of equations. Thus finding analytical expressions for temperature is generally not possible due to the complexity of the geometry and bondary conditions [43]. Therefore, computational methods are preferred, even less precise (approximate values).

Among different methods of analysis, the finite element method is a very accepted and commonly used method for thermal analysis. In this thesis, a finite element software is used. Therefore, only finite element method will be explored.

3.2.1 Finite Element Method (FEM)

The finite element method is a numerical mean to determine approximate solutions for partial differential equations (PDE) on a defined domain (W) [42]. Finite element consists of domain discretization into interconnected finite elements to create a thermal model. Thus, in each element the governing equation is approximated by any of the traditional variational methods [44].

A numerical model for satellite heat transfer starts with the definition of the physical problem. Besides this, the model can be divided into the discretization of the domain and the discrete approximation of the partial differential equations (PDE). Lastly, combining both, the numerical solution is obtained [43].

The basis for thermal analysis is the heat balance equation, which is based on the principle of energy conservation [43]. The heat balance equation expressed in Cartesian coordinates is given by

$$\rho c_p \frac{\partial T}{\partial t} = \frac{\partial}{\partial x}\left(k_{xx}\frac{\partial T}{\partial x}\right) + \frac{\partial}{\partial y}\left(k_{yy}\frac{\partial T}{\partial y}\right) + \frac{\partial}{\partial z}\left(k_{zz}\frac{\partial T}{\partial z}\right) + Q \tag{3.21}$$

where the thermal conductivity, k, can be expressed as

$$k = \begin{bmatrix} k_{xx} & k_{xy} & k_{xz} \\ k_{yx} & k_{yy} & k_{yz} \\ k_{zx} & k_{zy} & k_{zz} \end{bmatrix}$$

Equation 3.21 can be used to solve heat conduction problems in anisotropic materials with

directional variation in thermal conductivity.

3.2.2 Boundary and Initial Conditions

Before stating any analysis it's necessary to state appropriate boundary and initial conditions. Thus, a solution for the heat conduction equation is possible. The boundary conditions can be divided in two types or a combination of both, as can be seen in Figure 3.6. The first, the $Dirichlet$ condition, in which the temperature on the boundaries is known and/or the $Newman$ condition, in which the heat flux is imposed [43].

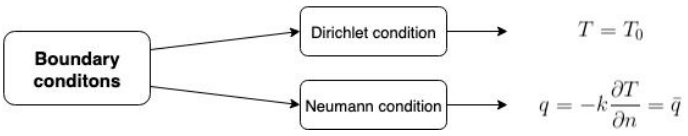

Figure 3.6: Boundary conditions.

The insulated, or adiabatic and the symmetry conditions are obtained with $\bar{q} = 0$ [43].

3.2.3 Linear Steady-State Heat Transfer Problem

In steady state calculations, the heat flux entering the satellite and the heat flux leaving are constant. Furthermore, material properties such as the conductivity are linear.

Figure 3.7: Heat flux across an insulated bar.

A simple heat conduction example in a laterally insulated uniform bar with a cross sectional area A and thermal conductivity k is shown in figure. Considering the Fourier heat conduction equation and the boundary conditions, the heat balance equation at the nodes are [45]:

Node 1:

$$Q = kA\left(\frac{T_1 - T_2}{L_1}\right) = \frac{kA}{L_1}T_1 - \frac{kA}{L_1}T_2 \tag{3.22}$$

Node 2:

$$Q = kA\left(\frac{T_2 - T_1}{L_2}\right) = \frac{kA}{L_2}T_2 - \frac{kA}{L_2}T_1 \tag{3.23}$$

The above equations can be rewritten in matrix form as:

$$\begin{bmatrix} \frac{kA}{L_1} & -\frac{kA}{L_1} \\ -\frac{kA}{L_2} & \frac{kA}{L_2} \end{bmatrix} \begin{Bmatrix} T_1 \\ T_2 \end{Bmatrix} = \begin{Bmatrix} Q_1 \\ Q_2 \end{Bmatrix} \tag{3.24}$$

Or as the main finite element equation [42]:

$$[K_c]\{T\} = \{p\} \tag{3.25}$$

where $[K_c]$ is the conductivity matrix, $\{T\}$ is an unknown nodal temperature and $\{p\}$ is the thermal load vector, which is the sum of the power due to heat flux at boundary $\{PB\}$ and the power vector related to the internal heat generation $\{PQ\}$. The system of equations is computed to find nodal temperatures $\{T\}$ [42]. After the nodal temperatures are calculated, the temperature gradients $\{\nabla T\}$ are calculated according to the element shape functions. Finally the element fluxes can be obtained by:

$$\{f\} = [k]\{\nabla T\} \tag{3.26}$$

Generally a realistic analysis of a thermal design for a satellite must be based on transient problem. In this type of analysis the system changes with time. Therefore, a transient analysis will result in the satellite temperature history over time [27].

3.3 Thermal analysis of nano-satellites

The design of thermal control system is divided in three sections. Firstly, the satellite configuration and orbit should be analyzed, and the equipment and structure temperatures should be predicted. Secondly, when the temperatures of the satellite's subsystems are outside of the operational temperatures, methods to control heat paths, improve dissipation or enhance heat generation, should be proposed. Finally, the thermal model should be tested and the results compared to the predicted ones [5].

Several modeling techniques are used on thermal analysis of CubeSats. Commonly software available in the market used for thermal design include: lumped parameter methods (ESATAN (ThermXL), SINDA/G/FLUINT, TRASSA), finite element and finite difference methods (NASTRAN, COSMOS, ANSYS, FLOTHERM, TAS, TAK2000) and radiation heat exchange (ESARAD, TERMICA, TRASYS, RadCAD, SSPTA, OAZIS) [46]. Several thermal analysis performed to CubeSats are summarized bellow.

Garzon in 2012 [47], using time-dependent computer FEA models, performed the thermal analysis of OSIRIS-3U. The software used was COMSOL Multiphysics®. Berggren in 2015 [36], performed a thermal analysis of the MIST 3U CubeSat using Siemens NX™. In 2016, for the same satellite, was developed a detailed thermal model using SYSTEMA/THERMICA [48].

Flecht in 2016 [37], created a model of PICSAT and performed several simulations using SYSTEMA/THERMICA. Kang and Oh in 2016 [30], used Thermal Desktop, SINDA/FLUINT and RadCAD to develop the on-orbit thermal analysis of STEP Cube Lab. The results obtained for the worst cases were then validated through a thermal vacuum test and the correlated thermal mathematical model with higher reliability was created.

Mason et al [25] implemented the thermal model for MinXSS in C&R Tech's Thermal Desktop software. Then the model was compared and tuned with the temperatures measured in the thermal balance vacuum testing. Finally, the model was validated comparing the predicted temperatures with actual on-orbit measured temperatures,which had an agreement within a few degrees Celsius.

SatTherm is a simple and easy software tool based in excel and Matlab. When compared with Thermal Desktop, the predicted values for the PharmaSat satellite were within 4ºC or less. This tool although is not powerful as other CAD based software it allows thermal analysis for the early stages of small spacecraft [49].

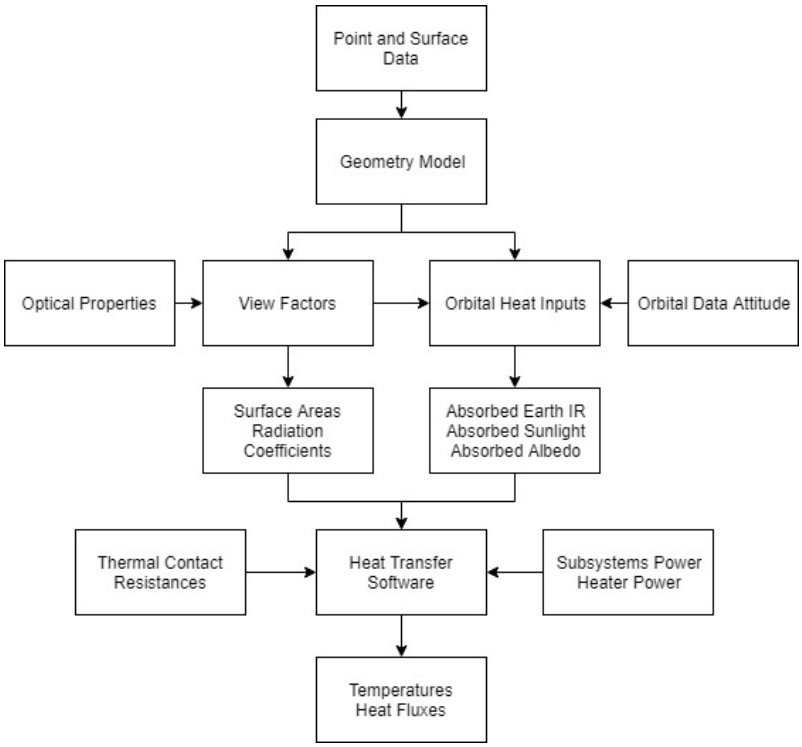

Figure 3.8: Flowchart of the design process and analysis of TCS.

In general, thermal analysis are performed using a finite element method implemented by a computer software. These programs transform the spacecraft into a mesh and compute the heat transfer between the nodes. The boundary conditions are given by the external heat loads. Thus the heat is conducted through he mesh. In each node it is possible to know the temperature and therefore heat fluxes.

Figure 3.8 show a simplified method of the design process and analysis of the thermal control system. Firstly, a geometric model of the spacecraft is generated with a computer-aided design (CAD) program. The level of the detail depends upon the level of development of the spacecraft and the level of analysis pretended. Critical components such as sensitive payloads, batteries and electronics should have a greater detail.

After the spacecraft is modeled, surface and material properties are applied to each volume section. Afterwards, the orbit and attitude data are used to compute transient external heat

fluxes. Finally, the software computes the temperatures and fluxes for each node.

Thermal analysis of a small satellite is a iterative process. It is performed at the start of a new design and then assess the adequacy of the thermal control systems. Changes should be performed if any component is outside of it's operational range and a new analysis should be repeated [21].

Since the simulations by themselves are not reliable they have to be experimentally validated. Therefore, thermal testing must be performed with an entire satellite or representative experiments to validate the methodologies used. In the following Chapters representative experiments of the main heat transfer mechanisms are performed to validate the current methodology.

Chapter 4

Experimental Study

This section describes the thermal tests performed, as well as, all the materials, equipment and procedures needed to complete the tests. The data acquisition system and vacuum chamber are described. At the end of this Chapter, test result temperatures are shown for all configurations and discussed. The results of the experiments will be used in the next Chapter as boundary conditions and as comparison results.

4.1 Experimental Study Description

The key objective of both experiments is to replicate the main boundary conditions (conduction and radiation)that a satellite withstands in space. The first experiment consists in analyzing the heat transfer by radiation between two aluminum plates. The second intend to quantify the thermal contact resistance between spacers and PCB. Both experiments are conducted in a controlled environment to simulate space environment conditions and minimizing convection effects. A schematic of the experiments in its test environment can be seen in Figure 4.1.

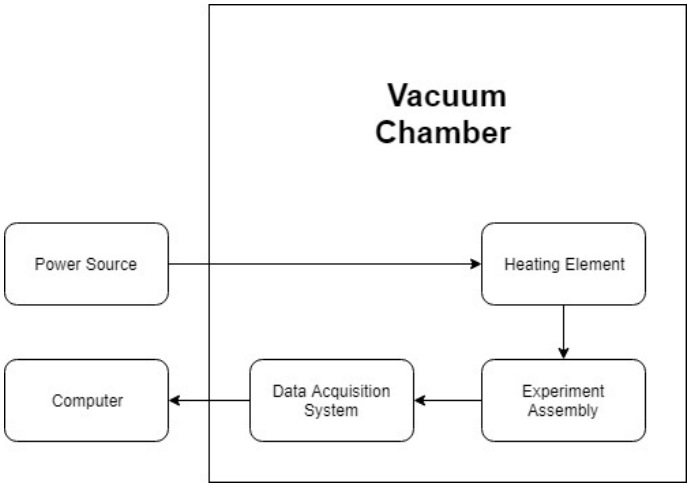

Figure 4.1: Overview of test set-up in the thermal vacuum chamber and data acquisition system.

Both test rigs were produced in CEiiA. The material was chosen according to both availability and costs. Both production methods and production technology was chosen considering the same premises. In each test, the experimental test rigs were placed inside the vacuum chamber alongside the data acquisition system. As the chamber was pressurized, the temperatures dropped abruptly, thus it was waited around ten minutes to stabilize all temperatures before powering the heating element. The heating element was powered on to provided the heat flux for each experiment accordingly. The temperatures were taken in specific points of the surfaces through the use of both thermocouples and data acquisition system. As soon as both

experiment reached steady state, the set of data acquired will be used for posterior analysis. Each test was performed three times to verify repeatibility between runs, increasing statistics. Both tests were conducted with different load cases and sensitivity studies were made to verify which configuration provided accurater measurements.

4.1.1 Radiation Experiment

The first experiment, intended to obtain the heat transfer through radiation between two aluminum plates with 100mm side. In different setups, the plates are separated by 20, 50 and 100mm. During the experiments one of the faces is heated by an infrared lamp connected to a regulated power supply. The lamp is positioned outside the chamber at a fixed distance and concentric with the plates. The other faces of the plates exchanged heat between them and surrounding environment. With these setups the view factors are expected to change between them, changing the heat fluxes and plate temperatures.

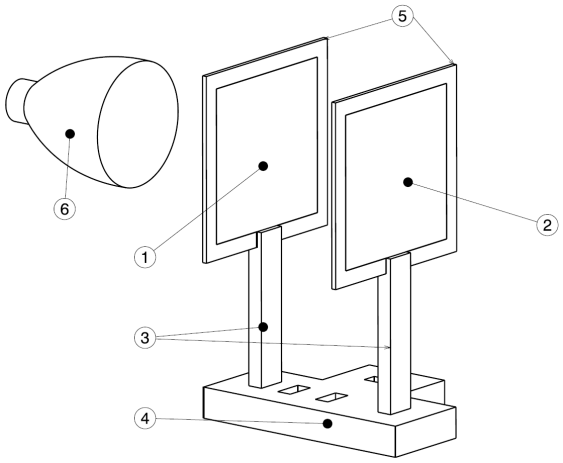

Figure 4.2: Radiation experimental test rig.

1 ⟶	First Plate
2 ⟶	Second Plate
3 ⟶	Vertical supports
4 ⟶	Main support
5 ⟶	Side cork insulator
6 ⟶	Heating element

Table 4.1: Label of Figure 4.2.

The test rig consists of a wood main support which holds vertical supports that in turn, hold both emitter and receiver, as can be seen in Figure 4.2. The main support has several holes that allow to place the plates at different distances. In order to simulate adiabatic conditions, all sides of the aluminum plates are insulated with cork. Apart from that, it is assumed that there are no heat transfer by conduction from the plates to the vertical wood supports due to the low conductivity of wood. Each plate was monitored with at least two thermocouples positioned at the middle and the corner of the plate.

Besides the different distance between plates, two types of lamps were tested, Figures B.2 and B.3. One was a ceramic infrared bulb with 100W and a diameter of 75mm. This lamp did not emit any light, thus has very high efficiency converting power into heat. Furthermore, the heat was distributed uniformly across the flat lamp face. The second lamp is a common incandescent infrared heat lamp with 150W and a diameter of 125mm, which emitted a red light. Both lamps were powered by a ceramic socket in a desk lamp support which allowed to adjust the position of the lamp relatively to the experiment.

Figures 4.3(a) and 4.3(b) shows the experimental rig positioned inside the chamber with both lamp configurations. Since the lamps were outside the chamber, it was constructed a funnel in

cardboard coated with aluminum foil to avoid heat dispersion. It also prevented unintentional heating of the second plate. The first lamp was inside this funnel and thus more protected from cooling by convection, lowering the eventual differences between consecutive runs. The second lamp was only leaning against the funnel more prone to convection cooling.

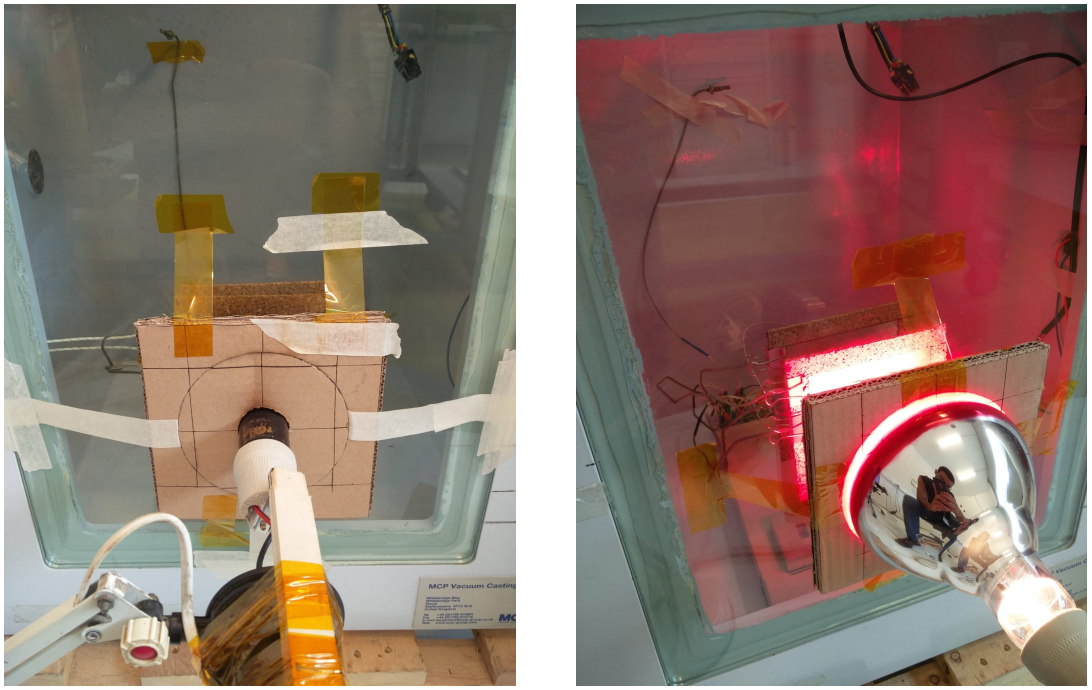

(a) 100W Ceramic bulb. **(b)** 150W Incandescent bulb.

Figure 4.3: Radiation experiment test rig inside the vacuum chamber with both lamp configurations.

4.1.2 Thermal Contact Conductance Experiment

The main objective of the second experiment was to study and estimate the thermal contact conductance between a PCB and a brass spacer, through an indirect method. As it was seen in Chapter 3, the determination of the thermal contact resistance is an extremely difficult task to do, specially in a CubeSat stack with small contact areas between spacers and PCBs. Several crucial parameters were unknown. Those parameters were the surface roughness, the mean asperity slope, the micro hardness and the pressure at the interface. Furthermore, without the knowledge of the actual temperature gradient across the interface it was impossible to determine the contact conductance h_c directly using correlations found in literature.

The chosen approach required that the measurements were taken at specific points in order to measure the overall temperature gradient and later use these measurements to derive the thermal contact resistance with the assistance of a thermal analysis software. Worth mention that this estimate is heavily influenced by some assumptions made such as the thermal conductivity of spacers and PCB.

Due to the foreseen difficulties, sensible studies were made and the best configurations were implemented. The test set-up was sought to be similar to a CubeSat PCB stack. However, the

available PCB was just 70X55mm (Figure B.1). Four tests were performed with two configurations with and without the use of nylon washers. In each spacer-nut or bolt-spacer assembly there are two contacts on both sides of the PCB. The use of nylon washers isolate thermally one of them. Figures 4.4(a) and 4.4(b) show both configurations.

The heat input is given by a soldering iron since it was the cheaper available solution. In a first assembly, the heat is conducted through the first spacer to the PCB and again to the second spacer. This test only forms one heat path. In a second assembly, the heat is distributed through two contacts in symmetrical positions of the PCB. If the heat flux passing through both contacts and the same load is applied, it is expected that both contacts present the same temperature differential across the interface. An aluminum plate is used as an heat sink to force an heat flux. This creates an heath path from the heat source through the spacers and PCB. The top side of the aluminum plate is insulated with cork to avoid heat exchange with the PCB. The bottom side is painted black to increase emissivity.

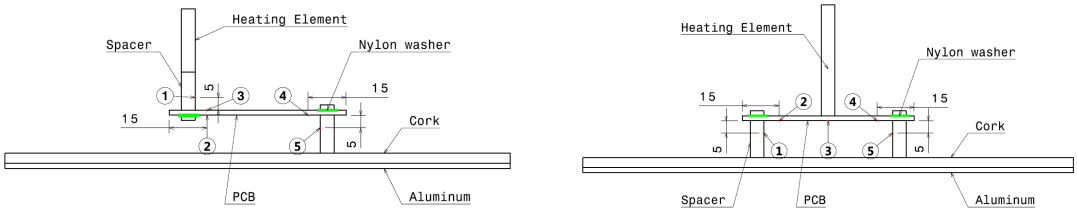

(a) Configuration 1. **(b)** Configuration 2.

Figure 4.4: Test set up schematics with the use of nylon washers. The numbers represent the location and position of the 5 thermocouples.

For the second configuration instead of four heat paths, as it seen in CubeSat stacks, only two were used. In the middle of the PCB it was drilled a hole to hold spacers and thus conduct the heat from the soldering iron to the PCB. Clips were used to restrict the thermocouple movement and prevent lifting. Figures 4.5(a) and 4.5(b) show the test rig assembly inside the chamber. A detailed view of the experiment without the measuring probes is shown in Appendix B.

4.2 Aluminum emissivity measure

The emissivity of aluminum plates is an unknown parameter with high influence in thermal analysis. Thus, it was performed a small experiment to estimate it and reduce the error associated with the use of a tabulated value. In order to measure the emissivity, the values measured from two thermocouples were compared with the measurements of an infrared camera FLUKE TiS45. Figure 4.6(a) shows the used setup and the taken image of the thermal camera (b). In the first place the temperature is measured with thermocouples. Afterwards, the emissivity value in thermal camera is adjusted accordingly, until it matches the temperature previously measured with the sensor. The measured temperature was compared with the half black painted side with an assumed emissivity of 0.9. The previous procedures were performed. It was estimated an emissivity of 0.4 for the aluminum plates in five different measures. This result indicates that the aluminum plates were heavily oxidized.

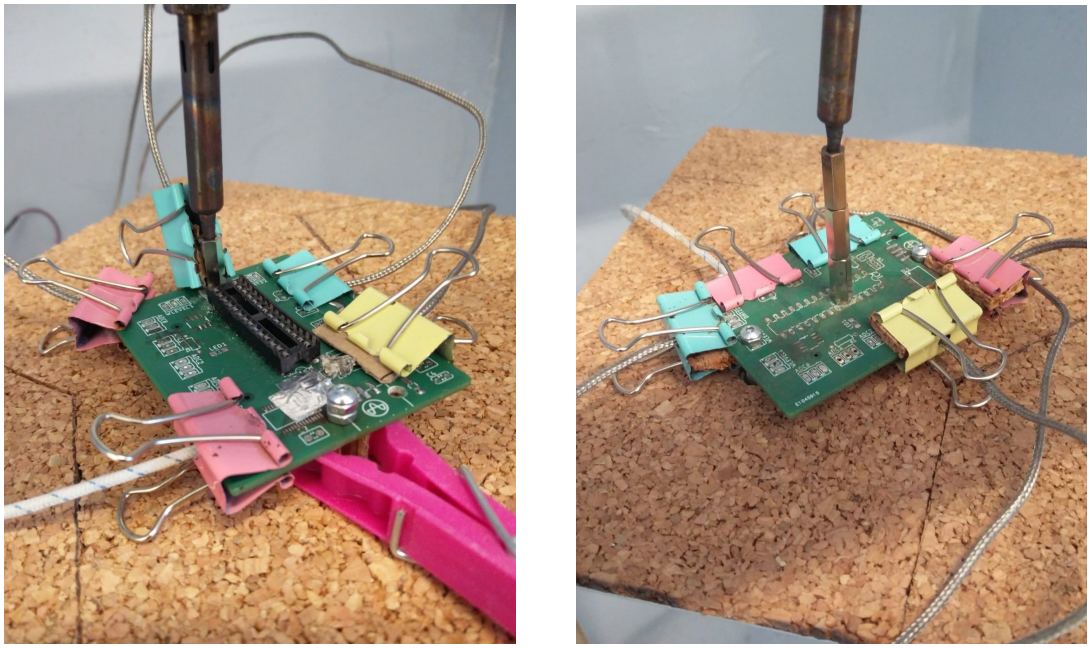

(a) Configuration 1. **(b)** Configuration 2.

Figure 4.5: Experimental test rig inside the vacuum chamber with instrumentation. The experimental rig is attached to the heat sink (aluminum plate covered by cork on the top).

4.3 Data Acquisition System

The data acquisition system is essential in any experimental test. The objective is to collect, process it and record data. Six thermocouples were used in these experiments with respective amplifiers, two Arduinos UNO and XBEE modules. Since it wasn't possible to pass the information to the outside of the vacuum chamber by cable, the gathered data had to be sent via a XBEE wireless link. The Arduino inside the vacuum chamber was powered by a 5V battery. Connected to the computer was a second Arduino which receives the data, exports and stores it in excel in real time for subsequent analysis.

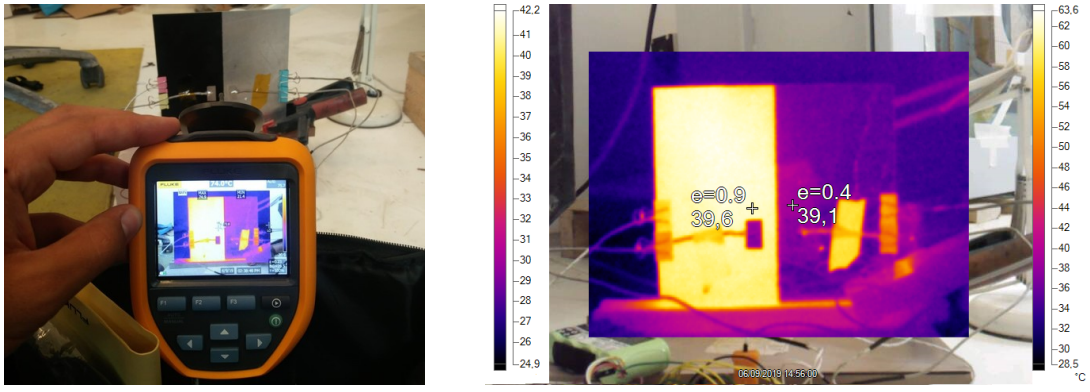

(a) **(b)**

Figure 4.6: Estimating the emissivity value by comparing the temperature measurement from thermocouple sensor with the value measure by the thermal camera.

There were several choices for measuring temperature: thermistors, silicon devices, and resistance temperature detectors. One of the simplest and cheapest is the thermocouple and it's also the device used in this project. A thermocouple is simply a junction of two dissimilar metals. The metallic junction creates a voltage, as illustrated in Figure 4.7. This phenomenon is called the Seebeck effect (discovered around 1821 by Thomas Seebeck). The voltage varies proportionately with temperature and the higher the temperature is, the higher the voltage will be [50, 51].

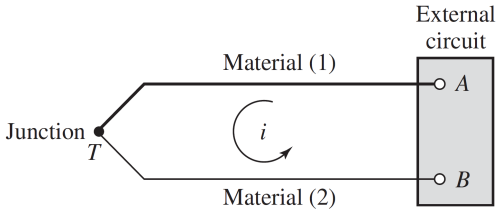

Figure 4.7: Seebeck thermoelectric effect [50].

Several different metal combinations are used to exploit the characteristic that different combination of metals creates different temperature increases to voltage increase ratio. Thermocouple types are referred to by using letters of the alphabet to denote the metal combinations used. One of the most common is a "K" type thermocouple, which is the type used in this work [51].

A significant problem arises with the fact that the voltage changes are very small and consequently very difficult to correctly convert to the actual temperature. In addition, it is necessary to determine not only the temperature of what is being measured by the thermocouple, but also the ambient temperature at the place where the voltage is being read.

There are several solutions to both of these issues, and one of the best and cheapest solutions are based on specialized integrated circuits. The MAX6675 integrated circuit is a product of Maxim Integrated. This converter reads the voltage from the thermocouple, amplifies it, and performs analog to digital conversion. It also performs cold-junction compensation and can read temperatures ranging from 0ºC up to 1024ºC with a resolution of 0.25ºC [52]. Figure 4.8 shows the complete assembly of the data acquisition system.

A major problem was faced while attaching thermocouples to flat surfaces and small areas. Several techniques combinations were tested. The method chosen was composed of aluminum foil tape and Kapton tape. Aluminum foil promotes a solid contact to the surface and the Kapton tape ensures adhesion. It was noticed that during heating the thermocouple could lift and give misleading readings, which occurred several times and ruined that data.

4.3.1 Calibration

Thermocouples like any other measuring device have associated errors and need to be calibrated. There are three main errors associated to the assembly used. An accuracy of ± 2.2ºC

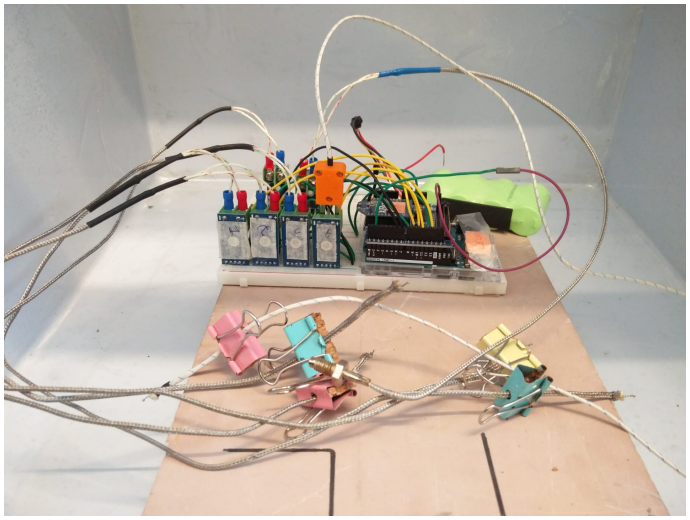

Figure 4.8: Data acquisition system assembly. Each thermocouple is connected to one amplifier.

for Type K thermocouples and the chip measurement error of ± 2.25ºC plus an additional Cold-Junction Compensation Error of ± 3.0ºC [52].

To minimize the error in the measurements the data acquisition system was calibrated accordingly to procedures suggested in [51]. Firstly, with ice and distilled water and secondly with distilled boiling water. In Figure 4.9 is observed both thermocouples. Caution was taken to prevent thermocouples from touching the bottom and the wall of the container. The first bath provided a temperature of 0.0ºC and the second one 100ºC. This process was done several times uploading a corrected code each time until all thermocouple temperatures matched.

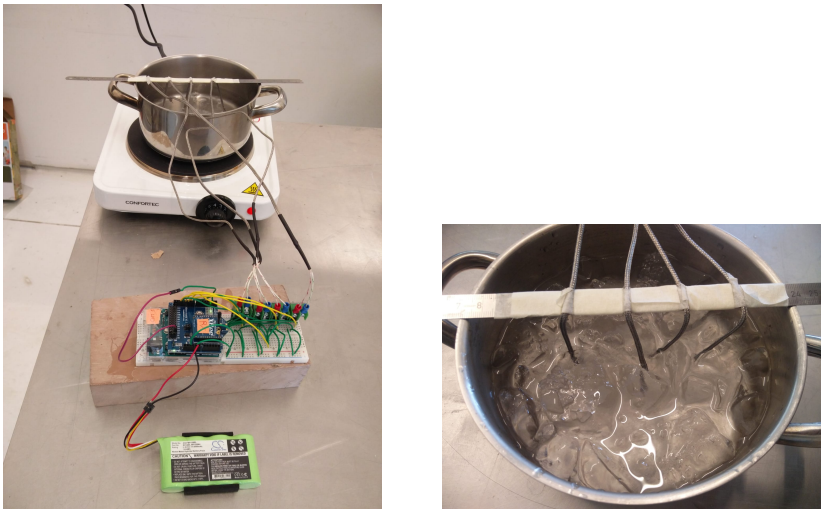

(a) Hot bath **(b)** Cold bath

Figure 4.9: Thermocouple calibration with two water points (a) hot bath, 100ºC and (b) cold bath, 0.0ºC.

It was verified high fluctuations in the readings because of thermocouples sensitivity and it's resolution of only 0.25ºC. Thus, it was implemented a exponential filter to the gathered data so it was easily identify the experiments reached steady state.

4.4 Test Vacuum Chamber Description

The vacuum chamber used in the experiments is an MPC Vacuum Casting System which allowed to reach pressure of 60 mbar during the complete test. This pressure level is considered a low/rough compared to actual vacuum of space (10^{-6} to 10^{-9} mbar) [53]. The chamber consisted in five metal walls painted white and a glass door with allowed the light beams to pass through. The vacuum chamber did not have a shroud to maintain a constant temperature in the walls. Thus, the temperature inside the chamber suffered changes during the experiment and during consecutive runs. Figure B.4 in Appendix B, shows a picture of the vacuum chamber used.

4.5 Experimental Results

After all the considerations presented previously, the experimental tests were performed. This section is divided int two subsections where the results are shown for each experimental test. The following tables and charts show the calibrated and processed measurements. Each test was repeated at least three times and the best test was chosen after a careful analysis of the processed data.

4.5.1 Radiative Parallel Plates

Tables 4.2 and 4.3 present the measurements for two different heating element configurations, as mentioned before. One with a Ceramic Bulb and other with an Incandescent Bulb. Plate 1 is the closest to the heating element, thus receiving all the incoming flux. Plate 2 is the one that is behind only being heated by the first plate. Represented by the D is the distance between plates. Additionally, during all test cases and runs the ambient temperature inside the chamber was monitored. Each table is followed by a respective graph, Figures 4.10 and 4.11, to better visualize and analyze the gathered data.

Table 4.2: Processed data of Ceramic Infrared Bulb experiment for the three different distances between plates.

	Temperatures [ºC]		
D [mm]	First Plate	Second plate	Ambient
20	114.75	64.125	29.25
50	101.50	41.375	28.50
100	100.00	38.375	31.00

Table 4.3: Processed data of Incandescent Bulb experiment for the three different distances between plates.

	Temperatures [ºC]		
D [mm]	First Plate	Second Plate	Ambient
20	168.50	78.25	31.00
50	157.00	50.50	30.00
100	158.25	40.00	30.50

As it can be observed, both tests show the same trend in all measurements. The plates temperatures decrease with the increasing distance between them. In Figure 4.10 it is possible to

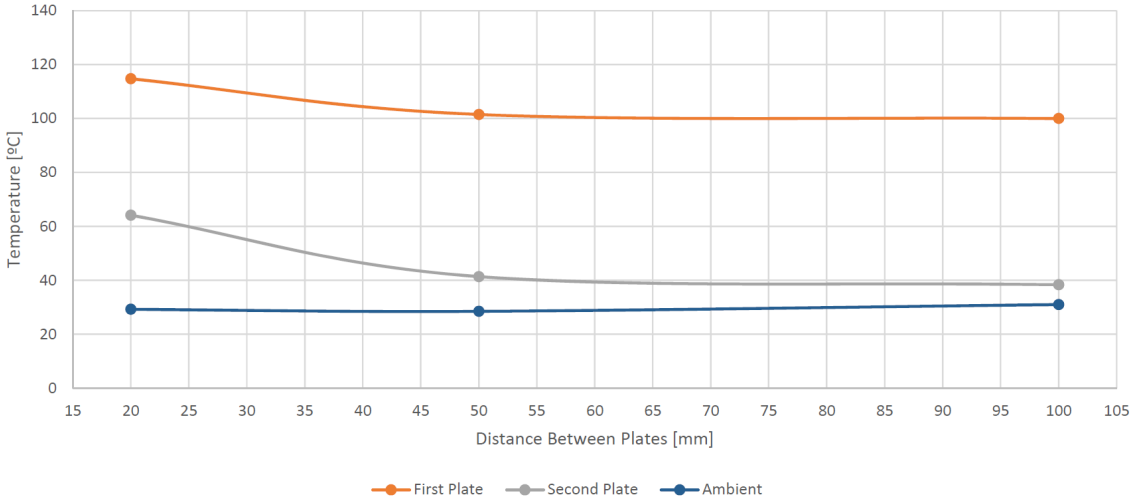

Figure 4.10: Plotted experimental data from the Ceramic Bulb experiment for each separation distance.

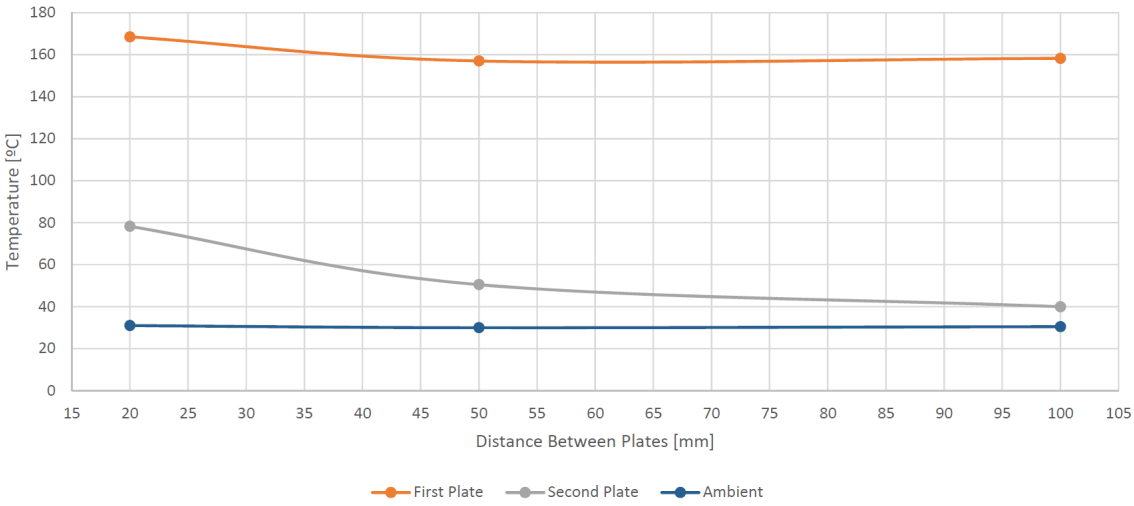

Figure 4.11: Plotted experimental data from the Incandescent Bulb experiment for each separation distance.

identify a value convergence from 50mm up to 100mm which goes with the predicted behavior. As the distance increases the view factors between the plates decrease from 0.7 up to just 0.2. In other words, a substantial amount of energy emitted by the first plate does not reach the second plate and is ”lost” to the ambient.

As expected, the higher temperatures were achieved with the Incandescent Lamp which has more power that the Ceramic Bulb, even at an higher distance from the first plate. Another observation worth mentioning, is the fact that the ceramic bulb took a longer time to reach a steady state temperature than the Incandescent one as can be observed in Appendix B which show all thermocouple measurements plotted as a function of time.

It was observed that a large area of the glass chamber door surrounding the funnel was really hot, suggesting that a quantity of heating flux was being absorbed by the glass and later re-emitted to the inside and outside the chamber.

As mentioned previously, the tests were repeated at least three times and it was noticed that

high deviations between runs were observed for the experiment with the Incandescent Bulb. This occurrence can be justified by the fact that the lamp was more prone to convection interference than the ceramic one. Add to the previously said, during the tests the room door was opened and closed several times. Throughout the day and consecutive days the ambient temperature outside the chamber fluctuated out of control (cooler temperatures during the morning and hotter temperatures during the afternoon).

It was verified that as soon as the Incandescent lamp was powered, it was possible to sense incoming flux whereas this was not occurring with the other lamp. The resistance took a longer time to heat but maintained it constantly after that.

4.5.2 Thermal Contact Conductance

The results are shown for the four configurations tested:

- Test 1: Configuration 1 with nylon washers;
- Test 2: Configuration 1 without nylon washers;
- Test 3: Configuration 2 with nylon washers;
- Test 4: Configuration 2 without nylon washers.

Tables 4.4 and 4.5 show the temperatures for both configurations. TC represents the number of the thermocouple measured. In Figures 4.4(a) and 4.4(b) the locations of each thermocouple are represented by the number circled. Thermocouple 6 was monitoring the ambient temperature inside the chamber.

Table 4.4: Experimental results of configuration 1.

	Temperatures [ºC]					
	TC_1	TC_2	TC_3	TC_4	TC_5	TC_6
Test 1	131.5	87.8	91.7	39.2	32.7	26.8
Test 2	118	90.8	96.7	39	33.5	27.7

Observing the results of table 4.4, it is verified that the temperature gradient across both contacts is higher for the configuration 1 than for configuration 2. The first contact ($TC_1 - TC_2$) presents a difference of 39.8ºC and 21.3ºC, in each test, which is almost half. It is clear the effect of isolation through the use of washers. The second contact ($TC_4 - TC_5$) presents once again an higher difference for the case with washers. However, the difference is lower, which indicates that the washers were not isolating.

As expected, TC_1 reached higher temperatures for the test with washers, since there is just one contact by which the heat flows. Thus, the heat is accumulated in the first spacer which indicates the solution didn't had time to converge to a more stable solution. Additionally, it is observed a gradient across the PCB ($TC_3 - TC_2$) of 4ºC and 6ºC. These results support the fact that the thermal conductivity is much more smaller through the plane than across the PCB.

Supposing there were no heat losses to the environment and the spacers were fastened with the same torque, it was expected that the temperature gradient across both contacts, in each test, would be the same. However, this was not verified, which means that the PCB loses a lot of heat by radiation (emissivity=0.89) and the heat fluxes across the contact are different.

Table 4.5: Experimental results of configuration 2.

	Temperatures [ºC]					
	TC_1	TC_2	TC_3	TC_4	TC_5	TC_6
Test 3	43.1	51.9	109.2	57.8	45.7	28.6
Test 4	41.3	53.5	78.9	57.9	45	30.8

Test 3 presents gradients across both interfaces very different, 8.8ºC and 12.1ºC, which suggests that in one interface the washer was not isolating. In Test 4 the drop across the interfaces obtained are near, about 12ºC and 13ºC. Considering, that the temperatures obtained in test 3 and test 4 for the thermocouples TC_4 and TC_5 are similar it might be caused by similar heatings and dissipations.

It is noticed a difference of $\pm$ 4ºC in locations were was expected temperature symmetry (TC_2 and TC_4). Furthermore, the same temperature drop across the contacts was expected, in the the case the PCB conductivity was isotropic and the spacer fasten torque were the same.

It observed that the gradient across a contact is significant and thus a crucial parameter in accurate thermal analysis, together with a deep characterization of all used materials. I was noticed that the use of nylon washers isolated thermally the contact, producing higher gradients across the interface. Thus it was concluded that the heat flux across the contact was reduced due to the less contacting area.

Several problems arose during the the thermal contact conductance experiment. It was observed that thermocouples lifted easily and suffered high variations between runs.

It is not possible to compare directly all tests, because in each test the spacers were unscrewed and fastened without a torque wrench, accordingly to the configuration. It was also very difficult to try to fasten the spacers with the same torque for each test without the proper tools. Also, some thermocouples were attached over again when the changes were made or when was detected that the thermocouple lifted.

Another uncontrollable variable was the inconstant input heat flux. The fact that the soldering iron was removed between tests did not allow to guarantee the same input heat flux every test, since it was only touching the spacer.

Even though all difficulties felt while measuring the thermal contact resistance, the tests confirm the considerable temperature drops across contacts and the importance of studying them in depth.

Chapter 5

Numerical Study

This section presents the numerical study and its comparison with the experimental tests. An analytical analysis of heat exchange between parallel plates was performed. The same analysis was done numerically. Since it was not possible to measure the actual flux leaving the lamps, a second numerical analysis was made to estimate the necessary flux to reach the experimental temperatures. The fluxes were compared and conclusions were taken.

For the contact resistance experiment two tests were modeled and analyzed. Contact conductance was estimated matching the temperatures obtained numerically with the experimental.

5.1 Analytical Analysis

As mentioned in Chapter 3, in spite of analytical methods being not suitable for complex cases, they give accurate results for simple analysis. The proposed method consists in analyzing the heat exchanged between parallel plates at a specific distance. In this analysis the temperature of the second plate is the temperature unknown variable. The known variables are the first plate (T_1) and ambient temperatures (T_3), obtained in the experimental tests.

This analysis can be illustrated by a radiation network method which represent the physical experiment. To construct it, a "surface resistance", $(1-\epsilon)/\epsilon A$, is "connected" to each surface and a "space resistance" $1/A_i F_{ij}$ is positioned between radiosity potentials. This type of analysis is very similar to the methods of analysis used in dc circuit theory, applying also the Kirchoff's current law. In Figure 5.1 the resistances are identified and denoted by the symbol of resistance. Surface resistance are given by the surface emissivity and area. Space resistances include the view factor between areas.

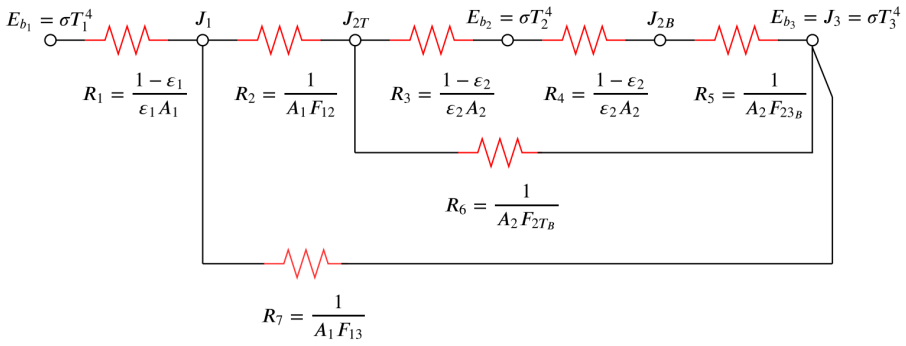

Figure 5.1: Radiation network for two parallel plates exchanging heat between them and an enclosure.

The network shown in Figure 5.1, is solved based on the fact that the net heat transfer, q, is the overall potential difference, $E_{b_1} - E_{b_3}$, divided by the sum of resistances. This principle is used

between all surfaces involved. Equations shown below summarize the methodology to solve the network. For resistance calculation is necessary to calculate the view factors between parallel plates. Analytical equations to calculate them are described in Chapter 2.

$$q = \frac{E_{b_1} - E_{b_3}}{R_{Tot}} \tag{5.1}$$

$$R_A = \frac{1}{\frac{1}{R_3 + R_4 + R_5} + \frac{1}{R_6}} \tag{5.2}$$

$$R_B = \frac{1}{\frac{1}{R_A + R2} + \frac{1}{R_7}} \tag{5.3}$$

$$R_{Tot} = R1 + R_B \tag{5.4}$$

To obtain the temperature of the second plate is necessary to calculate the radiosities as follows:

$$q = \frac{E_{b_1} - J_1}{R_1} \tag{5.5}$$

$$\frac{J_1 - J_{2T}}{R_2} = \frac{J_{2T} - E_{b_3}}{R_A} \tag{5.6}$$

$$\frac{J_{2T} - J_{2B}}{R_3 + R_4} = \frac{J_{2T} - E_{b_3}}{R_3 + R_4 + R_5} \tag{5.7}$$

Finally, using the previously calculated radiosities the emissive power of the second plate gives the overall temperature of the second plate.

$$E_{b_2} = \frac{J_{2T} + J_{2B}}{2} = \sigma T_2^4 \tag{5.8}$$

5.2 Software Description

A FEM analysis is divided into three elementary working steps: modelling (pre-processing), solution and vizualization of solution results (post-processing) [42]. The software used in this thesis for the pre-processing was Altair HyperMesh [54], the solver was MSC Nastran and the post-processing was Altair HyperView [55].

In general HyperMesh allows building FE models for third party solvers (non Altair), such as MSC Nastran, however it must be specified in HyperMesh. Some cards are not supported by HyperMesh and must be introduced by hand or through scripts.

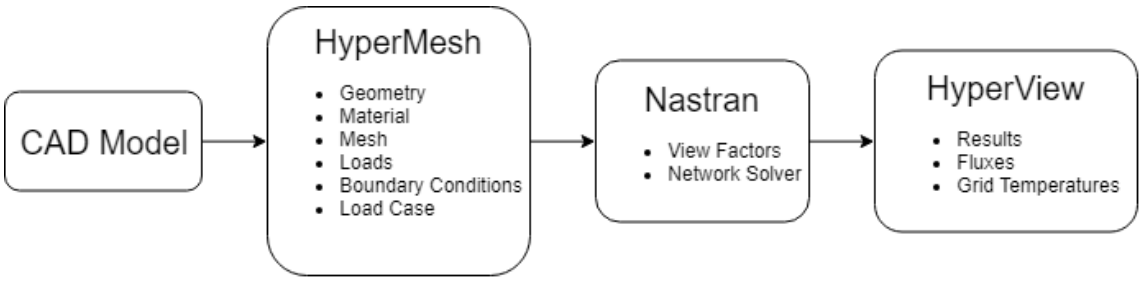

Figure 5.2: Process of FEM thermal analysis divided in pre-processing, solver and post processing.

Figure 5.2 illustrates the process of thermal analysis. The initial step is to import the component's CAD geometry into HyperMesh. After that, the model is divided into discrete elements and the properties of the model are defined (e.g material and surface properties, boundary conditions. After that Nastran is used to process the input file from HyperMesh and output a file for post-processing. Finally, the results are imported to HyperView for easier visualization and analysis.

NASTRAN (NAsa STRuctural ANalysis) computer program system was developed for NASA as a general-purpose computer program for analysis of the behavior of elastic structures using a finite-element method [56]. Posteriorly, heat transfer analysis capability was added based as well in finite-element method. The program has the ability to perform rendering temperatures distributions and heat flows in solid objects subjected to thermal boundary conditions. These boundary conditions comprise prescribed temperatures at grid points and specified thermal loads to convection and radiation in both steady-state and transient cases [57].

Using a program named "VIEW", Nastran is capable of computing the view factors and the required exchange coefficients between radiating surfaces [57]. These calculations can be the most computational intensive operation in heat transfer analysis.

5.3 Experiments Modeling, Meshing and Boundary Conditions

The following numerical analysis intent to compare and validate the methodologies used for thermal analysis. The objective is to model both experiments in HyperMesh and use the same loads. At the end of both analysis it is expected to obtain the temperatures in specific points. The boundary conditions were given by the experimental data in order to constraint the model. All components are meshed with 2D (CQUAD) and 1D (CBAR and CELAS2) elements for simplicity. CQUAD, CBAR and CELAS2 elements are conductive elements.

A three dimensional Cartesian coordinate system is used. In the thermal radiation analysis, Y axis is perpendicular to the plates. For the thermal contact conductance the PCB is placed int the XY plane.

5.3.1 Thermal Radiation Analysis

For the thermal radiation experiment the model consisted only by the two plates. The wood supports were disregarded due the low interference. It is assumed that the plates exchange heat only between them selves. The chamber walls are disregarded. The validity of this analysis is confirmed using HyperGraph, where the input heat flux is equal to the sum of output heat fluxes in the $.op2$ file.

The plates were aluminum, thus the following properties were used: a thermal conductivity of $167.9\ mW/mmK$ and an emissivity of 0.4 (measured experimentally). Figure 5.3 show the model meshed for a separation distance of $100\ mm$ between the plates.

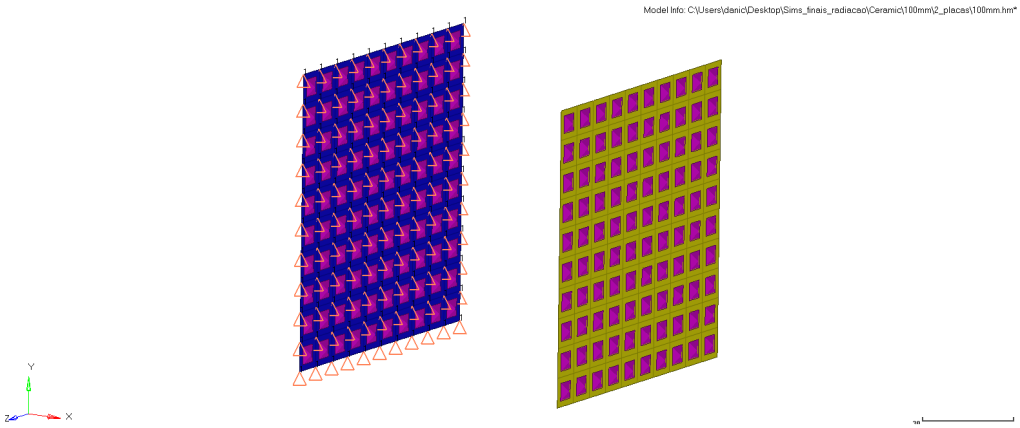

Figure 5.3: Thermal radiation between plates modeled in HyperMesh. Triangles represent the temperature constraints and the pyramids represent radiative elements (CHBDYE).

The pyramids in pink represent CHBDYE elements required for radiation thermal analysis. These elements control radiation properties. They inform which side of the plate (front or back) is emitting radiation and assign an emissivity (RADBC) to the surface.

In order to obtain the temperature of the second plate, first plate and the ambient temperature are constrained using the experimental data. These constraints are given as SPC's and are illustrated by triangles (Figure 5.3. For the different configurations the model is changed accordingly.

5.3.2 Contact Conductance Analysis

The contact conductance experiments were modeled similarly. Figures 5.4(a) and 5.4(b) show both configurations modeled. The PCB was approximated to a plate with same dimensions (70X55mm) and meshed with 2D elements (CQUAD). The assumed conductivity is equal to $k_{PCB} = 34.56\ mW/mmK$ as calculated in Chapter 6. The spacers were modeled with 1D elements (CBAR) with a hex cross sectional area and the properties of brass, $k_{brass} = 121\ mW/mmK$. The thermal contact resistance in both contacts were modeled with 1D elements (CELAS2). This element receives a property equivalent to the thermal conductance which is given by multiplying the contact conductance h_c by the contact area ($18.65mm^2$) and the number of contacts.

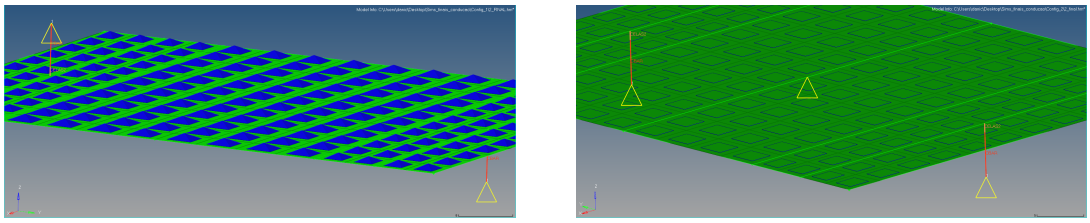

(a) (b)

Figure 5.4: Thermal contact conductance experiments modeled in HyperMesh. (a) Top side of Test 2 and (b) Bottom side of Test 4.

The test cases chosen to analyze were the Test 2 and Test 4 which have two contact points in each spacer-PCB link. These tests were observed to be the least influenced by external factors (the fact of the washers were probably not isolating). Thus, to constraint the model the temperatures used in this analysis were the temperatures measured in each test. In configuration 1, the temperatures of the first spacer (TC_1), the second spacer (TC_2) and the ambient were given to the model. For Configuration 2, the temperatures of both spacers and ambient were fixed. Additionally, the temperature in the middle of the PCB was set since the flux was given at that point.

5.4 Mesh Convergence Study

A essential step of while performing FEM analysis is verifying the adequacy of the mesh used. The mesh can be composed of elements in a triangular or quadrilateral shape. There are no fixed rules when choosing the type of mesh. It's known that for a type of element the accuracy increases with the decreasing element size. Furthermore, this mesh refinement is generally applied to regions where the temperature varies rapidly. Thus, engineers often begin with a simple finite element model and then use it to create a more refined model [58].

It was decided to analyze the results from two different meshes for radiation heat transfer between 100x$100mm$ plates. One mesh was composed of quads and the other of trias. The number of nodes was increased using sequential refined meshes. The same node was monitored across all refinements. Figure 5.5 represents the the mesh convergence study for the mesh composed of quads. It was verified that the two types of mesh delivered the same results with the same computational time consume.

5.5 Results

Several sensible studies were performed to develop the best methodologies to perform the desired thermal analysis. A great effort was put in comprehend the mechanisms of radiation heat transfer, simulate space thermal environment and methods to model the thermal contact conductance. Generally simpler models with 1D and 2D elements are seek. Despite that, it was

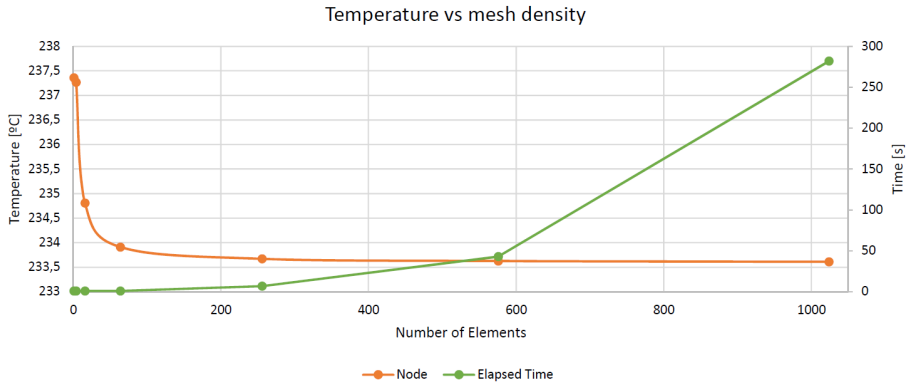

Figure 5.5: Quad element mesh convergence.

developed a methodology to model the thermal contact conductance. However, it was found that this methodology was rather time consuming to model. To simulate the enclosure (ambient) a CHBYP element was used with an SPC. This element acted as the ambient temperature.

Due to the low number of elements used the analysis were run quickly. The thermal radiation analysis only took 9s, while the thermal contact conductance analysis took 2s.

In the following section the results for both experiments are shown, compared with the experimental obtained and finally the results are discussed and conclusions made.

5.5.1 Thermal Radiation Analysis

It was observed that both analytical and numerical methods produced the same temperature results for the second plate. Figure 5.6 show the temperature distribution of the second plate for the case where the plates are separated by $100mm$ and heated by the ceramic bulb. Although, it seems there are different temperatures across the surface (Figure 5.6), the difference between the lowest and highest is 0.001°C. Thus, the temperature of the second plate is assumed uniform.

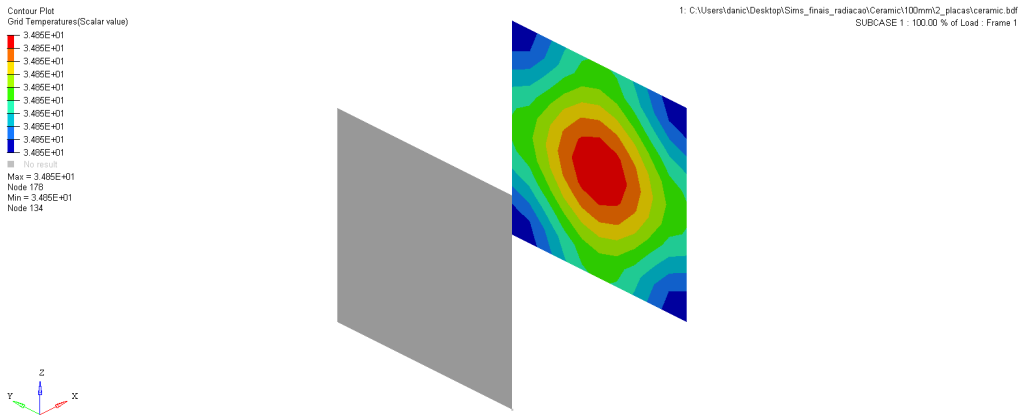

Figure 5.6: Thermal distribution of Plate 2 at distance 3 from the first plate.

As mentioned before, the first plate and ambient temperatures were fixed by the measurements given by the experimental data. Figures 5.7 and 5.8 show plotted temperature values for the second plate obtained by the three methods (Experimental, Numerical and Analytical, for the

Ceramic and Incandescent Bulb respectively. Also, a difference between both temperatures is plotted. Table 5.1 show the temperature of the second second plate and the associated error % between experimental and numerical results. The error analysis presented assumes perfect conditions in numerical analysis. This assumption will be discussed further ahead.

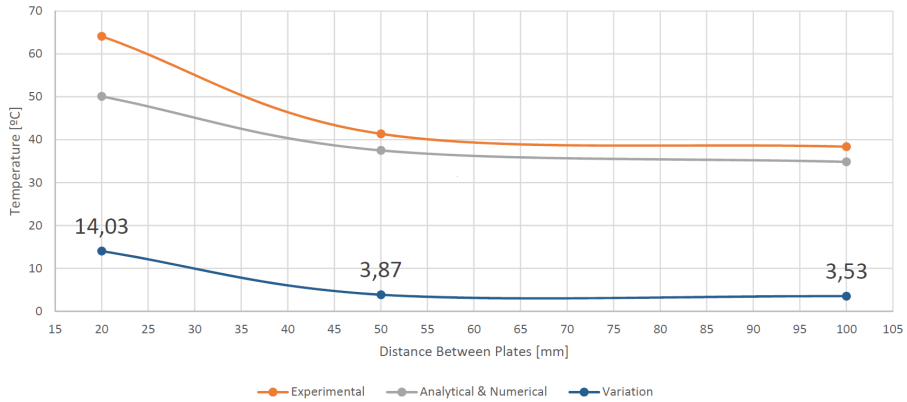

Figure 5.7: Temperature comparison between FEM analysis and Experiment 1 (Ceramic Bulb).

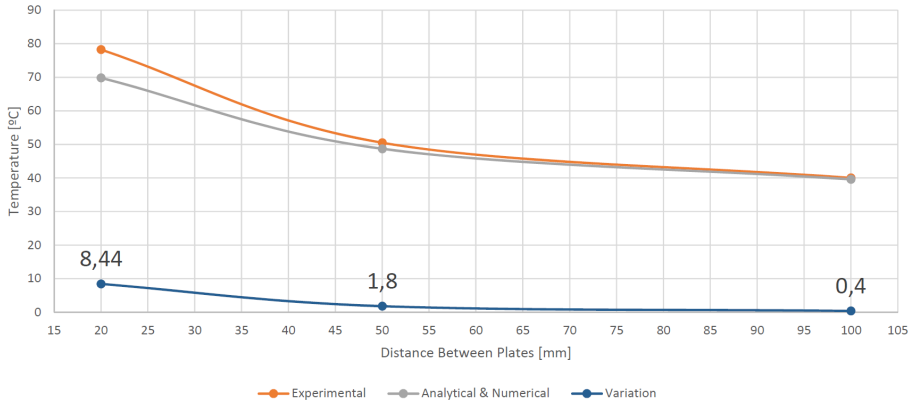

Figure 5.8: Temperature comparison between FEM analysis and Experiment 2 (Incandescent Bulb).

Table 5.1: Error % between experimental and numerical Results (Ceramic and Incandescent Bulb, respectively).

	Temperature [ºC]				Temperature [ºC]		
D [mm]	Experimental	Analytical & Numerical	%Error	D [mm]	Experimental	Analytical & Numerical	%Error
20	64.125	50.10	21.9	20	78.25	69.81	10.8
50	41.375	37.51	9.3	50	50.50	48.70	3.6
100	38.375	34.85	9.2	100	40.00	39.60	1.0

As can be seen in Figures 5.7 and 5.8, the temperatures Numerically obtained follow the same trend as the Experimental results. The temperature of the second plate decreases as the distance between the plates increases. This is supported by the fact that the view factors between the plates decrease as the distance between plates increases. Which means that less energy emitted by the first plate ”strikes” the second plate.

Furthermore, is clear that the variation between the experimental and numerical decreases as the distance between the plates increase. The Ceramic Bulb presents a maximum variation of 14ºC while the Incandescent 8.4ºC for the $20mm$ separation distance. This can be also observed in Table 5.1 where it is possible to identify an higher error associated to the ceramic bulb than for the incandescent bulb. These results reflect in a maximum error of 21.9% and 10.8% respectively.

The high errors associated to the distance of $20mm$, on both configurations, were associated to the fact that the glass heated in an area greater than the shadow of the first plate. Thus, the second plate was not only heated by the first plate, but also heated by the glass, contributing to the higher temperatures observed. The unwanted glass heating becomes less relevant since the view factors decrease as the distance between the second plate and the glass increases.

Another possible source of error could be the small size of the vacuum chamber, the fact that the walls were painted white and the low vacuum achieved by the pump. In the analytical and numerical analysis the vacuum is considered perfect and the enclosure is assumed as a black body at a constant temperature.

5.5.1.1 Effective Power Input Analysis

Further analysis was made to the experiment with the Ceramic bulb. These experiments proved to be more consistent. Also, it was possible to know exactly the area and distance that was emitting radiation whereas this was not possible with the Incandescent bulb due to the existence of a filament.

This analysis consisted in modeling a circle, representative of the bulb surface, in front of the two plates, as can be seen in Figure 5.9. The current was measured with a clamp-on-ammeter (72-7224 - Clamp Meter) which gave a result of 0.34 ± 0.025 A and a power consumption of 77.86W, which presents a significant difference compared with the rated power of 100W. It was not possible to measure the actual heat flux leaving the bulb due to several limitations. Therefore, this analysis intents to compare the power needed to reach the experimental temperatures for the first plate, against the actual power consumption. The same properties attributed before were used in this analysis.

Table 5.2: Power estimation results for all test configurations.

	Distance [mm]		
	20	50	100
Power estimated [W]	32.69	28.27	27.61
Power consumption measured [W]	77.86		

Firstly, examining the power estimations, it was observed that the heat fluxes necessary to achieve the experimental temperatures vary between test configurations. Which confirms, once more, the fact that the heat inputs between runs were inconstant. Another fact, is the big difference between the measured power and the power estimated. It is found that only 35/42%

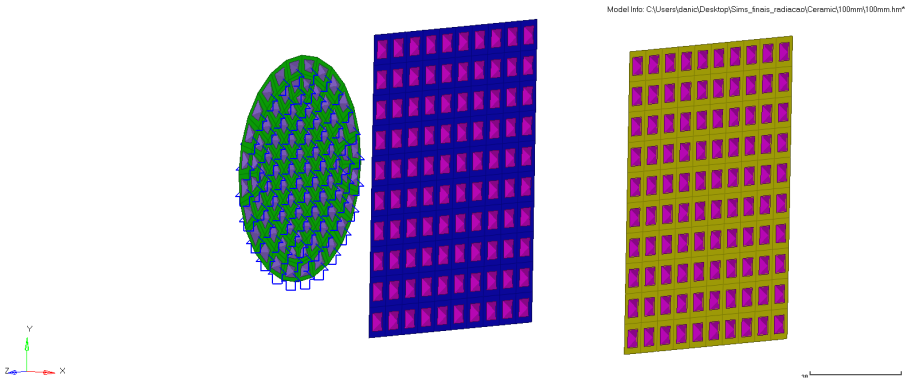

Figure 5.9: Model of the 100mm separation case.

of the consumed power is effectively being used to heat the plates, with a large quantity being dissipated to the surrounding environment.

With this analysis was observed that there is in fact a small temperature gradient between the center point and the corner in the order of 0.2ºC, for $100mm$ separation, up to 0.5ºC for $20mm$. This difference was not clear in the experimental data due to the low thermocouple accuracy.

5.5.2 Contact Conductance Analysis

The contact conductance analysis was performed and the results are show in Figures 5.10(a) and 5.10(b) for both simulations with a contact conductance $h_c = 80.4mW/mm^2K$. It is possible to verify the uniform temperature distribution across the PCB. Furthermore, different contact conductance were tested and the results are presented in table 5.3.

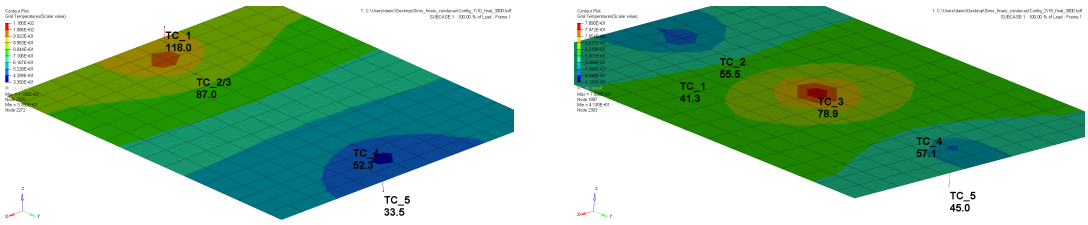

(a) (b)

Figure 5.10: Results obtained for both configurations with $h_c = 80.4mW/mm^2K$.

Observing the results obtained for both configurations is possible to verify that for configuration 2 there is a good agreement between the experimental and the numerical data. As for configuration 1, the results are significantly different. This discrepancy can be caused by uncounted losses in the numerical model or even different material properties assumed (conductivity and emissivity).

It is found that thermal contact resistance ranges between $h_c = 80.43^{+53.62}_{-53.62}\ mW/mm^2K$ remain within acceptable values. The resulting contact conductance range is compared to the values obtained by Hager in [38] for aluminum spacers without washers in a similar experiment. Hager

Table 5.3: Comparison between results obtained in experimental and simulations for both configurations.

		Configuration 1		Configuration 2	
	Experimental	90.8/96.7	39	53.5	57.9
CELAS2 [mW/K]	h_c $[mW/mm^2K]$	TC_2/3 [ºC]	TC_4 [ºC]	TC_2 [ºC]	TC_4 [ºC]
1000	26.81	85.4	52.7	56.4	57.9
2000	53.62	86.5	52.4	55.8	57.3
3000	80.43	87	52.3	55.5	57.1
4000	107.24	87.2	52.2	55.4	57
5000	134.05	87.4	52.1	55.4	56.9

obtained values of $h_c = 55.197^{+42.266}_{-19.534}\ mW/mm^2K$ which are in good agreement with the results obtained in the present measurements.

Although these values show an high uncertainty, they demonstrate the necessity of understanding the behavior of these stacks and the thermal impacts involved. Furthermore, they will allow to use reasonable assumptions for contact conductance when modeling CubeSat stacks in future thermal analysis.

Chapter 6

Thermal validation of 3-AMADEUS CubeSat

This section includes a brief description of the thermal modeling of 3-AMADEUS in HyperMesh. Extreme simulation cases are defined and explained as well as assumptions and simplifications made. The aim of the performed steady state analysis is not to give accurate temperatures, but rather apply the conclusions gathered from the experimental analysis and estimate initial temperatures of the main components. The necessity of changes in the thermal control system is evaluated.

6.1 3-AMADEUS Anatomy

3-AMADEUS is mainly composed of Printed Circuit Boards inside the main structure. The stack follows the PC-104 standards and is hold together by spacers. The various subsystems used are the On Board Computer (OBC ABACUS), transceiver (Nano Dock DMC-3), antenna system (ISIS Antenna), magntorquer (Nano Torque GST-600), batteries and electrical power system board (Nano Power P31u). Finally, the CubeSat is covered by solar cells to harvest energy from the sun and power the several subsystems. All these components are off the shelf and readily available. Figure 6.1 displays the entire satellite without the solar panels mounted.

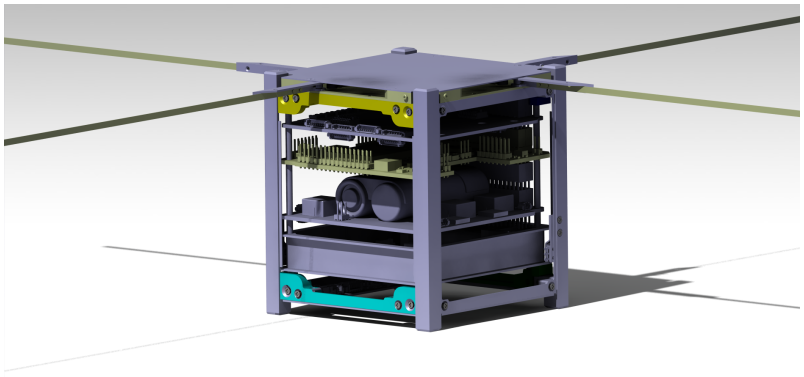

Figure 6.1: 3-AMADEUS concept structure and main subsystems.

6.2 Thermal Requirements

The current thermal design of 3-AMADEUS consists in a heater connected to a thermostat. The heater is positioned on the batteries and can dissipate up to 3W. 3-AMADEUS components and critical operation temperatures are outlined in Table 6.1 and were taken from component data sheet. Structure and aluminum panels are assumed to withstand temperatures ranging from

Table 6.1: Operational temperatures of 3-AMADEUS components and internal heat dissipation in both worst case scenarios. The orbit is considered at an inclination of $i = 0$.

	Operational Temperatures [ºC]		Internal Dissipation [mW]	
Component	T_{min}	T_{max}	Cold Case	Hot Case
Solar Cells	-55	125	0	0
OBC ABACUS	-45	85	50	650
NanoPower P31u	-40	85	160	160
Batteries	-40	85	3000	5
Nano Dock DMC-3	-40	85	0	208
Nano Torque GST-600	-40	85	0	809
ISIS Antenna	-20	60	0	40

-100ºC up to 100ºC.

6.3 Simulation Cases

The thermal analysis are carried by computer simulations in MSC NASTRAN. One limitation of this software comes with the fact that the full lifetime of one year is impossible to be simulated due to high simulation time. Therefore, only the extreme cases are simulated individually in a static & non-linear heat transfer analysis. For the spacecraft thermal analysis two worst cases were defined: a hot case and a cold case as can be seen in Figure 6.2. They represent a combination of the orbit parameters and altitude, which result respectively in the highest and lowest incoming fluxes incident on the satellite. Other possible orbits would receive a flux between these two and thus the thermal requirements would be guaranteed to be fulfilled.

Several assumptions were made in order to maintain the analysis low time consuming. Due to the uncertainty in orbital parameter, it is assumed that the CubeSat is in a circular orbit at around 550km of altitude. Furthermore, the CubeSat is assumed to not be tumbling and always with the same orientation towards the Earth's center. As can be seen in Figure 6.2 one face always points towards Earth while the other points in the direction of travel.

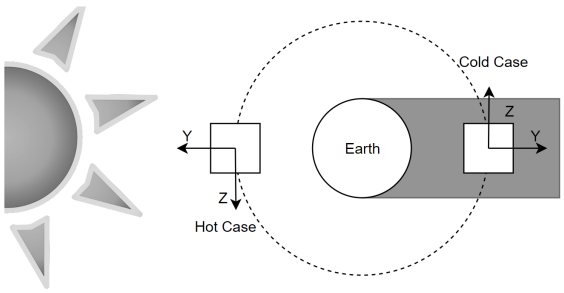

Figure 6.2: Representation of the considered worst case cold and hot with an orbit with .

Additionally, the satellite is heated by the dissipation of the electronics inside the satellite when in operational or safe modes. Table 6.1 also show the heat dissipated by the internal components for both cases. This internal dissipation is distributed across all surface of the modeled component. MSC Nastran do not compute the external heat input upon the surfaces in

a specif orbit. Therefore, the solar radiation, Earth Albedo and Earth IR had to be calculated with the equations presented in Chapter 2. In addition, view factors between satellite surface and Earth had to be derived for planet and albedo radiation. Considering the study case and for surfaces whose normals are parallel to and perpendicular to the local vertical vector, the view factors can be computed respectively by:

$$F_{\parallel} = \left(\frac{r_e}{r_e + h}\right)^2 \tag{6.1}$$

$$F_{\perp} = \left(\frac{1}{2\pi}\right)\left[\pi - 2sin^{-1}\left(\sqrt{1 - \left(\frac{r_e}{r_e + h}\right)^2}\right) - sin\left(2sin^{-1}\left(\sqrt{1 - \left(\frac{r_e}{r_e + h}\right)^2}\right)\right)\right] \tag{6.2}$$

where r_e is Earth's radius and h the orbit altitude [59].

6.3.1 Hot Case

The hot case corresponds to the conditions that causes the highest temperatures the satellite will be subjected in orbit. It is characterized by the highest incoming fluxes of solar radiation and Earth IR radiation simultaneously. As was seen in Chapter 2, the highest solar flux occurs when Earth is closest to sun, which is at winter solstice and corresponds to a solar heat flux of $1.4129 mW/mm^2$. At the same time, the internal dissipation is considered at its maximum, with all electronics and instruments operating and dissipating as much energy as possible as can be seen in Table 6.1.

6.3.2 Cold Case

Generally, the cold case occurs when Earth is furthest from the sun, at aphelion in summer solstice. Other characteristic of this case is that the satellite has the longest possible transit through eclipse, which means, at some point it do not receive any flux from the sun. However, considering it is impossible to simulate this time of orbit, it was chosen to consider the eclipse as the worst case scenario. In eclipse, the satellite only receives flux coming from the Earth IR. Moreover, it is assumed that the internal dissipation in minimal and the satellite is in a non operational state. The batteries are assumed to be dissipating 3W because of the heater incorporated.

6.4 Thermal Model

Due to the early development of the satellite the model was kept very simple in order to obtain a first estimation of the expected temperatures. Several simplifications and assumptions were made to the structure. Despite the fact 3D elements make a component with much more detail, it was chosen to model all components besides the battery with 1D and 2D elements to lower the computing time.

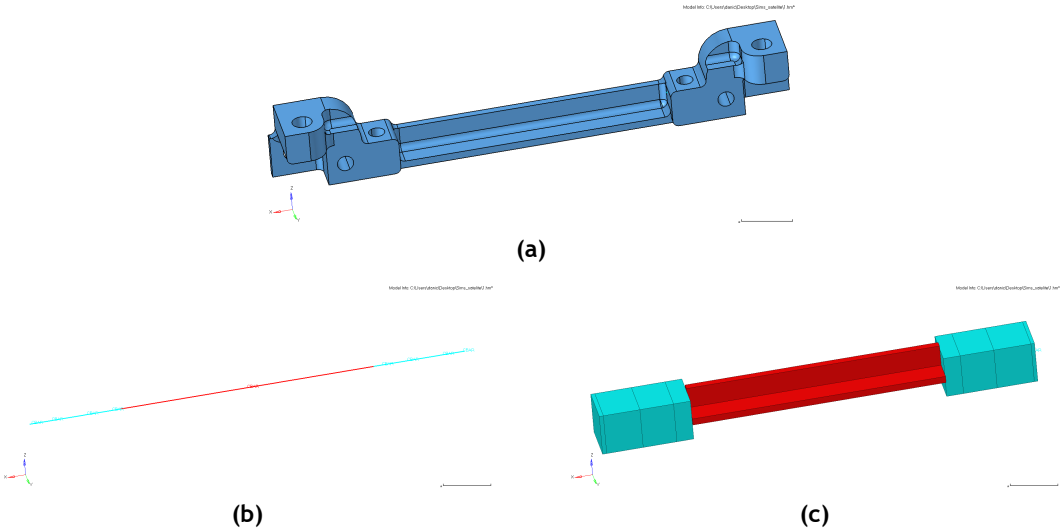

Figure 6.3: Comparison between CATIA 3D model and the 1D modeled rib in HyperMesh with the detailed 1D representation.

Starting with the structure, all round and chamfered edges were removed. The main rails were approximated to a L section composed of 2D elements (CQUAD), mainly because rails pose an important conductive element and it contributes to radiation exchange with the interior and the exterior.

All four Ribs were modeled with 1D elements. Figure 6.3 show the comparison between the Ribs modeled in CATIA and HyperMseh. Due to its geometrical complexity it was considered easier to model with 1D elements (CBAR) ignoring thermal radiation exchange with other components. It was assumed these elements would only conduct heat between rails and to the solar panels. Using the functions of HyperBeam, the central piece of the rib was considered as an L section with same size. The sides were approximated with cubical sections. Firstly, the total volume of the RIB was measured in CATIA and then the central L section volume was subtracted. With the obtained volume and with the length of the sides, an equivalent area was determined.

The solar cells/solar board and the PCB's were considered as plates with small thickness. Thus were modeled with 2D elements. All edges and small details were removed. Only the batteries were modeled with 3D elements (CHEXA), because it was component with the higher volume.

The adequacy of the mesh was verified in the past Chapter.The same results obtained in the mesh convergence study were applied to the current model.
Table 6.2 summarizes the thermal properties of all 3-AMADEUS components incorporated to the model.

6.4.1 PCB Thermal Conductivity

Most of the electronics of a CubeSat is composed of Printed Circuit Boards. Thus the thermal behavior and thermal properties of PCBs must be understood. PCBs are made of layers of FR-4 and copper similar to laminate composites and must be correctly modeled. FR-4 has a low con-

Table 6.2: List of material thermal properties for 3-AMADEUS CubeSat.

Component	Material	Emissivity ϵ	Absorptivity α	Thermal Conductivity mW/mmK		
ISIS Antenna, Nano Dock DMC-3, OBC ABACUS, Nano Power P31u, Solar Panel	FR4 Fiberglass	0.89	0.8	Planar 34.56	Normal 0.34	[60, 61]
Structure	Anodized Aluminum 6061	0.14	0.84	167.9		[62]
Batteries	Lithium Ion	0.25	0.4	24.8		[63]
Nano Toque GST-600	Plastic	0.89	0.89	0.4		[62]
	Cooper	0.03	0.03	392.2		

ductivity on the other hand copper has an high conductivity, therefore it is expected that the conduction within the plane to be greater than he conductivity through the plane.

The thermal conductivity is dependent on the number of copper layers the stack consists of, the thickness of the copper layer and the total thickness of the PCB. One simple way of modeling the thermal conductivity, without modeling each layer, is to determine the actual thermal conductivity values. Based on experimental measurements [60, 61], the expressions to estimate the different conductivities, in plane (planar) and through-plane (normal), are given by:

$$k_{planar} = 385\frac{h_{Cu}}{h} + 0.87 \tag{6.3}$$

$$k_{normal} = \left[3.23\left(1 - \frac{h_{Cu}}{h}\right) + 0.0026\frac{h_{Cu}}{h}\right]^{-1} \tag{6.4}$$

where h_{Cu} is the total thickness of the copper layers and h is the total thickness of the PCB. Usually the PCB are composed of four copper layers with a thickness of $35\ \mu m$ each and a total thickness of $1.6\ \mathrm{mm}$. The solar boards are composed of only two layers with $70\ \mu m$ and a total thickness $1.6\ \mathrm{mm}$. The resulting thermal conductivities are: $k_{planar} = 34.5575\ mW/mmK$ and $k_{normal} = 0.3393\ mW/mmK$. These vales have been used as average material properties for the thermal model of the CubeSat 3U-AMADEUS .

6.4.2 Conductive Links

The conductive links are important components of thermal analysis. They are composed of all screws that connect the solar cells to the ribs, the screws that connect the ribs to the main structure and finally the spacers that connect the PCB's between them and to the structure. All these links were modeled with 1D elements more properly elements CELAS2. This type of element accepts a conductivity equal to the resistance of the link. Thus, being independent of the element length.

Firstly, for the screws links, it was used values from the literature. The screws considered are M3 which gives a correspondent bolted joint conductance of $263.85mW/K$ [19]. For the PCB's

stack it was assumed a contact resistance of $80.43mW/mm^2K$ as it was estimated in the previous Chapter. Along with contact resistance, it was added a spacer linear conductor resistance calculated wit the cross sectional area, brass conductivity and spacer length.

Figure 6.4 shows the completely assembled CubeSat meshed in HyperMesh. Solar panels were removed in order to achieve a better view of the inside components.

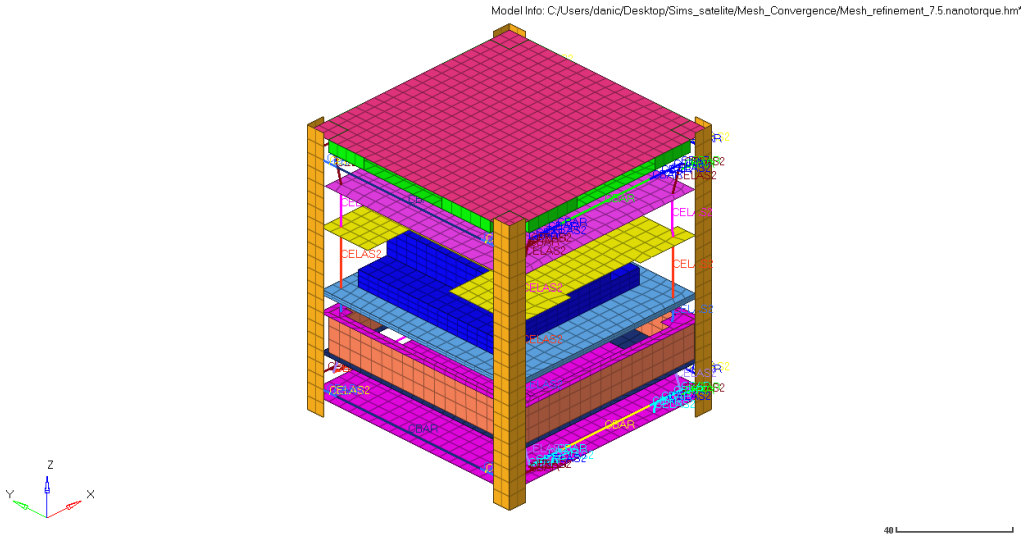

Figure 6.4: Meshed 3-AMADEUS CubeSat without solar panels.

6.5 Results

Both numerical analysis were performed. Although, low time consuming analysis were seek, the run time for both cases was half an hour.

The results from the simulations are shown in Figure 6.5. The graph displays the temperature ranges that the components are subjected in hot and cold cases. These temperatures include an uncertainty of 10ºC to account for modeling errors, as stated in ECSS standards. Operational temperatures are also displayed in order to better evaluate if a component exceeds its required range.

In the cold case the internal components temperature vary between -55.5ºC up to -30ºC while in the hot case these temperatures vary between 9.6ºC and 27.2ºC. It is observed that for the Hot Case, all temperatures remain comfortably inside the limit ranges. However, these results show that for the cold case many temperature limits are exceed, specially the ISIS antenna.

The reason why these components do not meet the requirements may be fact that the analysis performed is steady state. This is not the case of a satellite in orbit which is continually heating and cooling down. Furthermore, the satellite experiences eclipse only a small portion of the whole orbit. As the CubeSat orbits from direct sunlight to eclipse area, the component temperatures are slowly cooling down. Therefore, they may not cool down completely up to the temperatures obtained in the steady state analysis performed. Another fact that might be

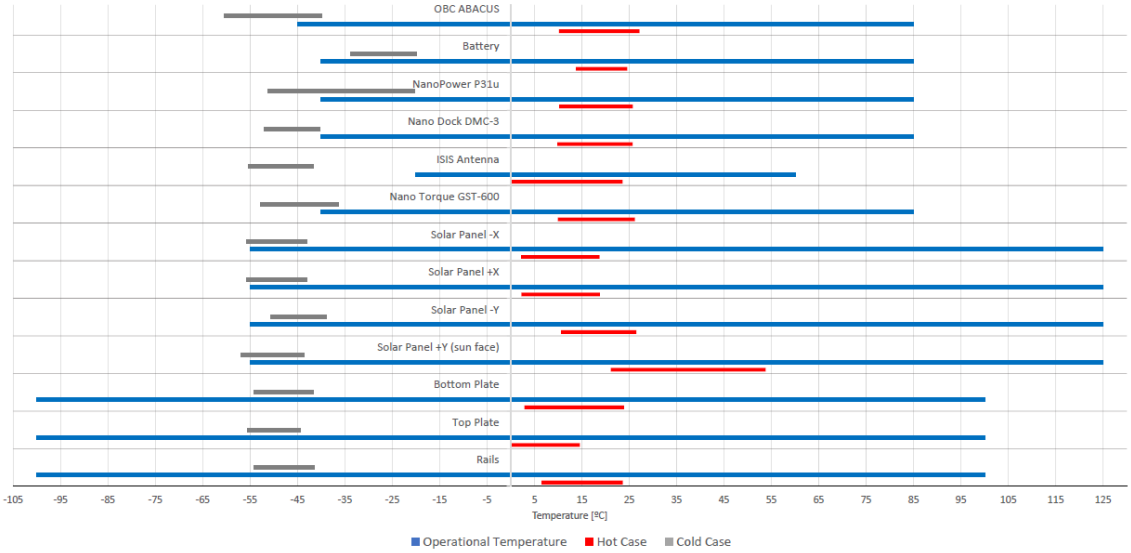

Figure 6.5: Temperature ranges for hot and cold case along with operational temperatures.

contributing to lower temperatures is the fact that in the simulated configuration the CubeSat, is covered by solar panels besides the top and bottom, which have an high emissivity and thus lose too much heat to the environment.

Due the limiting circumstances and since this is only a preliminary analysis it is suggested to implement small modifications to the thermal control system to make sure it withstands the cold case. The thermal design is driven by the limited mass and power budget. Thus, to increase the temperature of the satellite, the TCS must rely on passive methods of thermal control such as linking the battery to colder components through copper wire and covering the satellite inside by an isolating material. Aerogel could be a good option to apply in the satellite's inside walls, due to its lightness and ultra-low conductivity. The absorptivity of the sun pointed face could be improved to raise the satellite temperatures prior entering the eclipse. Ultimately in the case of need, using heaters is vital for survival.

Chapter 7

Conclusions

7.1 Overview

The main goals of this thesis was to gain confidence when performing thermal analysis, validation of the methodologies used in thermal analysis and validation of the current thermal control system of 3-AMADEUS CubeSat. It involved understanding the basic principles behind thermal analysis and thermal control of satellites. With the elaboration of this work, it was possible to experimentally test the two main heat transfer methods present in spacecrafts, in order to validate the current methodologies used for thermal analysis. Research and development of test rigs have been presented. The results obtained were compared with the Numerically analysis.

The first experiment consisted of radiation heat transfer between two aluminum plates, varying the distance between them and the heating element used. Regarding the distance between the plates, as expected, the plates reached higher temperatures for the smaller distance ($20\,mm$). Is was observed that the temperatures decreased as the distance between them increased, which confirms the fact that the view factors were reduced and thus an amount of energy leaving the first plate did not reach the second plate and was lost to the environment. When comparing the numerical results with the experimental measurements, it was verified that the second plate experimental measurements were higher than the expected. This deviation reflected in a maximum error of 22% between both analysis. The higher temperatures verified in the experimental measurements could be induced by unwanted heating of the glass chamber door and other uncontrollable and limited conditions. Regarding the different heating elements, it was concluded that the incandescent bulb provided closer results to the expected than the ceramic bulb. However, the last provided more consistent measurements between consecutive runs of the same test.

For the thermal contact conductance it was verified, as expected a significant drop in temperature across the contact between spacers and PCB's. In order to estimate the contact conductance, it was chosen an indirect method approach. Several configurations were tested in order to evaluate which one provided the best results. A numerical model of the experiment was constrained using the experimentally measured values. Temperatures were taken at specific points and compared with the predicted ones. It was concluded that the contact conductance between brass spacer and PCB without washers ranged from 26.81 up to $134.05\ mW/mm^2$. Worth mention that the values obtained are highly dependent on the thermal properties assumed. Furthermore, it was not possible to correlate with existent empirical equations due to the unknown numerous properties such as the bolt pressure, surface roughness, micro hardness. Although it was not possible to obtain an exact measurement of the contact conductance, the estimations obtained in this work, present a good agreement with past literature measurements.

It can be concluded that the results obtained in both experiments, in general, presented a good agreement. The methodology used for thermal analysis was validated and the results obtained can support and present a contribution for the CubeSat developers. Several modifications can be made to improve Experimental and Numerical results in order to improve thermal tests, as it will be discussed further ahead.

Finally, a preliminary steady state thermal analysis was performed to 3-AMADEUS CubeSat. This analysis did not mean to be too exhaustive, but rather provide first estimation for the temperatures experienced in orbit during the worst case scenarios and implement the current validated methodology for thermal analysis. The conclusion of the analysis, was that the satellite would survive the hottest case, however the temperatures obtained with the cold case exceeded the operational temperatures. In order to increase the feasibility of the project, it was recommended to implement passive thermal control methods such as using aerogel in the interior of the spacecraft due to its high thermal insulation.

7.2 Constraints and Challenges Experienced

Despite the fact that the aim of this study was validation of numerical simulation with the experimental, test rigs and experimental procedure were undoubtedly, the phase where most of the difficulties occurred. Some issues were found when performing the experiments. Many were solved, however several were not possible to overcome, like the fact that the glass door protecting the vacuum chamber was heating, the unsteady temperature inside the chamber, the impossibility to maintain the same input heat flux in every experiment and ultimately the uncertainty associated to the data acquisition system. The solution adopted was to construct a cardboard funnel to try to limit the glass heating and maintain a constant heat input, however this option was not well succeed.

Firstly, tests to measure contact conductance are quite difficult, especially for the small surface areas involved in CubeSat applications. Working with thermocouples and attaching them to surfaces proved also a very challenging task, with several lifting during runs. It was tricky to place the small thermocouple head in a specific point and glue it in place. It was found that a combination of aluminum tape and Kapton tape solved most of the problems. Moreover the use of tabulated material properties greatly limited the accuracy of the numerical analysis.

Considering the thermal contact condutance experiment, Configuration 2 results (Table 4.5) present one temperature reading that was not expected, which means the thermocouple eventually lifted. Thermocouple TC_3 in test 4 presents a difference of 30ºC, which do not follows the trend of the others thermocouples that present similar temperatures between both tests.

Regarding the acquisition system it was found high fluctuations during readings, which were solved with an exponential filter. Capacitors were implemented as suggested by the amplifier manufacturer, however no improvements were noted. Also when the data acquired was being written in excel several times the wireless system failed and corrupted data was written. This caused some loss of data and delay when processing it.

3-AMADEUS CubeSat thermal analysis also presented some challenges as the software used for this dissertation could not compute the input fluxes across an orbit and count with possible tumbling. Therefore, it was only possible to perform steady state studies.

7.3 Open points & Future Work

The work performed in this thesis can be improved and continued in several aspects. For instance, other tests could be done with the same experimental rig. In the case of thermal radiation experiment, several options could be tested, such as, either varying the material and surface properties, evaluating the presence of shadowing or the presence of a radiation shield and varying the view factors with the plates hinged at 90º. Improvements to the facilities should also be considered, such as, performing the experiments in a larger thermal vacuum chamber to minimize the influence of the enclosure. A constant temperature inside the chamber is crucial for more accurate measurements.

Concerning the contact conductance, several improvements can be made, starting with fastening the spacers with the same torque, controlling the input power using electric controlled heaters with similar power input as the ones seen in CubeSat applications. A torque wrench or a Fugifilm prescale cell should be used to measure the pressure. Surface properties should also be characterized, surface roughness with an optical interference microscope or surface profiler and the Microhardeness with a Vickers microhardeness measurement tool. Also, the test set up should be involved in MLI to reduce loss of heat by the spacers and PCB to environment. Future applications also could evaluate the presence of interstitial material to reduce the thermal contact resistance if necessary.

In relation to the data acquisition system other more expensive alternatives could be studied. K-type thermocouples present higher uncertainty than T-type. Also, the last is more suitable for vacuum environments. Besides that, the amplifier used is considered obsolete. Recently newer amplifiers have been developed by MAXIM Integrated such as the MAX31856, which presents a resolution of 0.0078125ºC and an accuracy better than $\pm$ 0.7ºC [64].

Considering, 3-AMADEUS project is still in a conceptual phase. Hence, many details are unknown. Thus the preliminary thermal analysis chosen was just steady state. However, steady state analysis means that the temperature and heat flux at a node in the CubeSat model, will not change with time. However, this is not true. Fluxes vary constantly during the whole orbit. Thus, in order to obtain more accurate and realist temperatures, the author suggests preforming a transient analysis of several orbits with specific thermal analysis software such as ESATAN-TMS, which is a standard European thermal analysis tool.

Bibliography

[1] J. Wertz, D. Everett, and J. Pushell, *Space Mission Engineering: The New SMAD (Space Technology Library, Vol. 28)*. Microcosm Press, 2011. 1, 6, 7

[2] J. Bouwmeester, M. Langer, and E. Gill, "Survey on the implementation and reliability of cubesat electrical bus interfaces," *CEAS Space Journal*, 2017. 1

[3] B. S. Matisoff, *Handbook Of Electronics Packaging Design and Engineering*. Springer Netherlands, 2012. 2

[4] S. May, "What is a satellite?" 2015, accessed: 2019-02-27. [Online]. Available: https://www.nasa.gov/audience/forstudents/5-8/features/nasa-knows/what-is-a-satellite-58.html 5

[5] P. Fortescue, G. Swinerd, and J. Stark, *Spacecraft Systems Engineering*. John Wiley & Sons, 2011. 5, 6, 7, 11, 12, 24

[6] D. Millard, *Satellite: Inovation in orbit*. Reaktion Books, 2016. 5

[7] UNOOSA, "Online index of objects launched into outer space," 2019, accessed: 2019-02-27. [Online]. Available: http://www.unoosa.org/oosa/osoindex/search-ng.jspx?lf_id=5

[8] "Posat-1," accessed: 2019-02-27. [Online]. Available: https://www.infopedia.pt/apoio/artigos$posat-1 5

[9] M. Lusa, "Corrida espacial 14 consórcios internacionais querem lançar satélites dos açores," 2018, accessed: 2019-02-27. [Online]. Available: https://24.sapo.pt/atualidade/artigos/ariane-virgin-e-roscosmos-na-corrida-ao-porto-espacial-dos-acores 6

[10] "satellite mass categories," accessed: 2019-03-17. [Online]. Available: http://www.daviddarling.info/encyclopedia/S/satellite{_}mass{_}categories.html 6

[11] W. A. Shiroma, L. K. Martin, J. M. Akagi, J. T. Akagi, B. L. Wolfe, B. A. Fewell, and A. T. Ohta, "Cubesats: A bright future for nanosatellites," *Central European Journal of Engineering*, 2011. 6, 8

[12] S. Lee and R. Munakata, "CubeSat Design Specification (CDS)," 2016. 7, 14

[13] A. Toorian, K. Diaz, and S. Lee, "The CubeSat approach to space access," *IEEE Aerospace Conference Proceedings*, vol. 1, 2008. 7

[14] D. Selva and D. Krejci, "A survey and assessment of the capabilities of cubesats for earth observation," *Acta Astronautica*, vol. 74, 2012. 7

[15] N. C. L. Initiative, "Cubesat 101: Basic concepts and processes for first-time cubesat developers," p. 96, 2017. 8, 14

[16] "Ecm-space." [Online]. Available: https://www.ecm-space.de/index.php/launch-adapters-h/cubesat-sizes 8

[17] K. Nakaya, K. Kazuya, S. Hirotaka, U. Kyoichi, O. Hideto, M. Naoki, I. Masafumi, U. Tomoyuki, Y. Nobumasa, K. Munetaka, O. Kuniyuki, M. Ikutaro, M. Saburo, and T. Robert, "Tokyo tech cubesat : Cute-i," *21st International Communications Satellite Systems Conference and Exhibit AIAA*, 2003. 8

[18] "Nanosats database," accessed: 25-02-2019. [Online]. Available: https://www.nanosats.eu/#database 8, 9

[19] D. G. Gilmore, *Spacecraft Thermal Control Handbook, Volume I: Fundamental Technologies*. American Institute of Aeronautics and Astronautics, 2002. 9, 10, 12, 13, 14, 16, 17, 18, 53, 65

[20] ECSS, "Space engineering: Space environment (ecss-e-st-10-04c)," 2008. 9, 10, 11, 13, 14

[21] J. Meseguer, I. Pérez-Grande, and A. Sanz-Andrés, *Spacecraft Thermal Control*. Elsevier Science, 2012. 9, 10, 11, 26

[22] S. Mills, "Earth albedo and emitted radiation," 1971. 10, 11

[23] E. Agasid, R. Burton, R. Carlino, G. Defouw, A. D. Perez, A. G. Karacalıoğlu, B. Klamm, A. Rademacher, J. Schalkwyck, R. Shimmin, J. Tilles, and S. Weston, *State of the Art Small Spacecraft Technology*, S. Weston, Ed. National Aeronautics and Space Administration, 2018. 12

[24] "Thermal control issues for nano- and picosatellites," in *57th International Astronautical Congress*. American Institute of Aeronautics and Astronautics, oct 2006. 12

[25] J. P. Mason, B. Lamprecht, T. N. Woods, and C. Downs, "Cubesat on-orbit temperature comparison to thermal-balance-tuned-model predictions," *Journal of Thermophysics and Heat Transfer*, 2017. 12, 13, 25

[26] R. Hon, C. Kesler, and D. Sigurdson, "Integrated testing of a complete low cost space cryocooler system," *International Cryocooler Conference*, 2009. 12

[27] R. Karam, *Satellite Thermal Control for Systems Engineers*. American Institute of Aeronautics and Astronautics, 2012. 13, 15, 16, 24

[28] E. T. T. Force, "Space engineering testing ecss-e-st-10-03c," European Space Agency, Tech. Rep., 2012. 13

[29] TEB, "Tailored ecss engineering standards for in-orbit demonstration cubesat projects," European Space Agency, Tech. Rep., 2016. 13

[30] S.-J. Kang and H.-U. Oh, "On-orbit thermal design and validation of 1 u standardized CubeSat of STEP cube lab," *International Journal of Aerospace Engineering*, 2016. 13, 24

[31] ECSS, "Space engineering: Thermal control general requirements (ecss-e-st-31c)," 2008. 13, 14

[32] J. P. Holman and S. Bhattacharyya, *Heat Transfer*, special in ed. McGraw Hill Education, 2008. 15, 16, 17, 18, 19, 20, 21

[33] L. J. Salerno and K. Peter, "Thermal contact condutance," NASA Ames Research Center, Tech. Rep., 1997. 16

[34] M. Yovanovich, “Four decades of research on thermal contact, gap, and joint resistance in microelectronics,” *IEEE Transactions on Components and Packaging Technologies*, 2005. 17

[35] C. V. Madhusudana, *Thermal Contact Conductance*. Springer International Publishing, 2013. 17

[36] A. Berggren, “Design of thermal control system for the spacecraft mist,” Master’s thesis, Kith Royal Institute of Technology School of Electrical Engineering, 2015. 18, 24

[37] T. Flecht, “Thermal modelling of the picsat nanosatellite platform and synergetic prestudies of circus nanosatellite,” Master’s thesis, Lulea University of Technology, 2016. 18, 24

[38] P. B. Hager, T. Flecher, K. Janzer, H. Brouwer, M. Jonsson, and L. L. Pérez, “Contact condutance in common cubesat stacks,” *49th International Conference on Environmental Systems*, 2019. 18, 47

[39] M. F. Modest, *Radiative Heat Transfer*. Elsevier LTD, Oxford, 2013. 19

[40] Y. A. Engel, *Heat and Mass Transfer: A Practical Approach*. McGraw-Hill, 2006. 20

[41] A. K. Oppenheim, “Radiation analysis by the network method,” *ASME*, 1956. 21

[42] M. Goelke, *Practical Aspects of Finite Element Simulation - A Study Guide*, ser. HyperWorks. Altair, 2015. 21, 22, 23, 24, 40

[43] P. Nithiarasu, R. W. Lewis, and K. N. Seetharamu, *Fundamentals of the Finite Element Method for Heat and Mass Transfer*. John Wiley and Sons Ltd, 2016. 22, 23

[44] J. N. Reddy, *An Introduction to the Finite Element Method*. McGraw-Hill Education, 2005. 22

[45] R. D. Cook, D. S. Malkus, M. E. Plesha, and R. J. Witt, *Concepts and Applications of Finite Element Analysis*. John Wiley & Sons, 2011. 23

[46] V. Baturkin, S. Zhuk, J. Vojta, F. Lura, B. Biering, and H.-G. Lötzke, “Elaboration of thermal control systems on heat pipes for microsatellites magion 4, 5 and bird,” *Applied Thermal Engineering*, vol. 23, pp. 1109–1117, 06 2003. 24

[47] M. M. Garzon, “Development and analysis of the thermal design for the osiris-3u cubesat,” Master’s thesis, The Pennsylvania State University, 2012. 24

[48] S. Chandrashekar, “Thermal analysis and control of mist cubesat,” Master’s thesis, Kth Royal Institute of Technology, 2017. 24

[49] C. Allison, M. Diaz-Aguado, and B. Jaroux, “Sattherm: A thermal analysis and design tool for small spacecraft,” *Conference on Small Satellites*, 2009. 25

[50] J. P. Holman, *Experimental Methods for Engineers*. McGraw-Hill, 2012. 32

[51] J. G. Webster and H. Eren, *Measurement, Instrumentation, and Sensors Handbook*. Taylor & Francis Ltd., 2017. 32, 33

[52] M. Integrated, “Cold-juntion-compensated k-thermocouple-to-digital converter (0ºc to +1024ºc),” Tech. Rep., 2014. 32, 33

[53] C. R. Tilford, *Physical Methods of Chemistry*. John Wiley and Sons, 1992. 34

[54] “Altair hypermesh,” accessed: 2019-07-08. [Online]. Available: https://www.altair.com/hypermesh/ 40

[55] “Altair hyperview,” accessed: 2019-07-08. [Online]. Available: https://altairhyperworks.com/product/hyperview 40

[56] T. G. Butler and D. Michael, “A summary of the functions and capabilities of the nasa structural analysis computer system,” *NASA SP-260*, 1971. 41

[57] H. P. Lee and J. B. Mason, “Nastran thermal analyser: A general purpose finite-element heat transfer computer program,” *NASA TMX-2637*, 1972. 41

[58] N. Ottosen and G. Peters, *Introduction Finite Element Method*. Pearson Education, 1992. 43

[59] S. L. Rickman, “A simplified, closed-form method for screening spacecraft orbital heating variations,” *NASA Johnson Space Center*, 2002. 51

[60] K. Azar and J. E. Graebner, “Experimental determination of thermal conductivity of printed wiring boards,” *Twelfth Annual IEEE Semiconductor Thermal Measurement and Management Symposium. Proceedings*, 1996. 53

[61] G. J. E. and A. K. K., “Thermal conductivity measurements in printed wiring boards.” *J. Heat Transfer*, 1997. 53

[62] T. L. Bergman, F. P. Incropera, D. P. DeWitt, and A. S. Lavine, *Fundamentals of Heat and Mass Transfer*. John Wiley & Sons, 2011. 53

[63] S. Chen, C. Wan, and Y. Wang, “Thermal analysis of lithium-ion batteries,” *Journal of power sources*, 2005. 53

[64] M. Integrated, “Precision thermocouple to digital converter with linearization,” Tech. Rep., 2015. 59

Appendix A

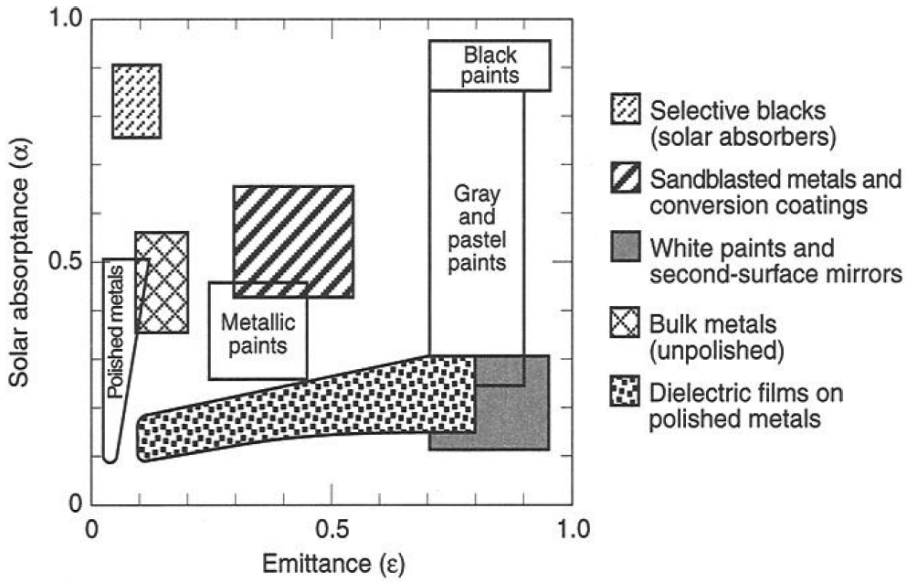

Figure A.1: Surface characteristics by type of finish [19]. The figure presents the emissivity and absorptivity for common finishes used in satellites

Appendix B

B.1 Test Rigs

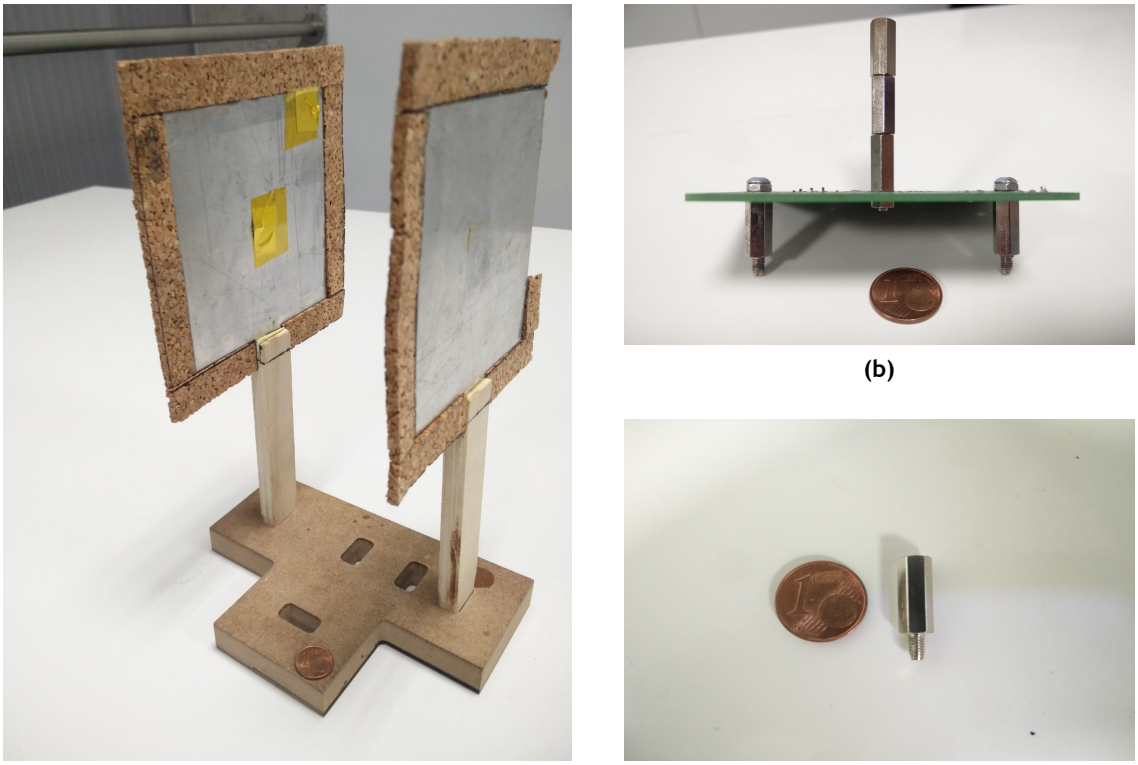

(a) (b) (c)

Figure B.1: Test rig details without thermocouples. (a) Radiation experiment (b) Configuration 2 conductance experiment (c) Brass spacer detail used in conductance experiments.

Figure B.2: Ceramic Bulb.

Figure B.3: Incandescent bulb.

Figure B.4: Vacuum chamber used to perform the experimental test. It provided the controlled environment desired. The convection heat transfer was minimized.

Appendix C

C.1 Radiation experiment thermocouple readings over time

This section presents the thermocouple readings over time for the radiation experiments. It is possible to verify that the Incandescent bulb reaches a steady state faster than the Ceramic bulb

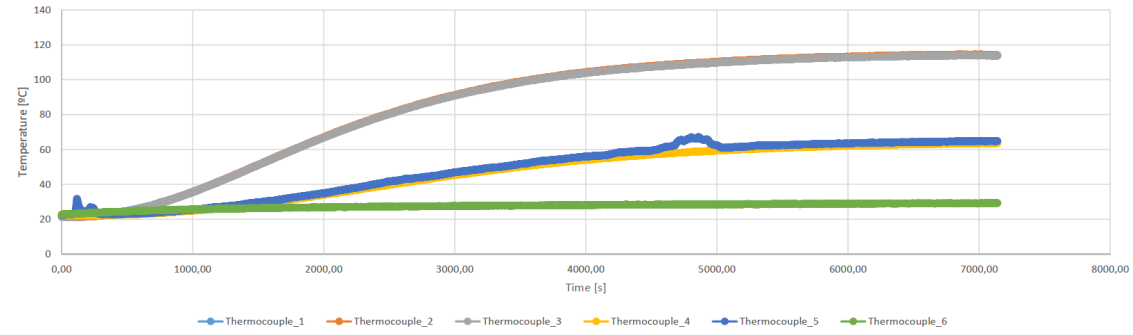

Figure C.1: Ceramic bulb, 20mm separation.

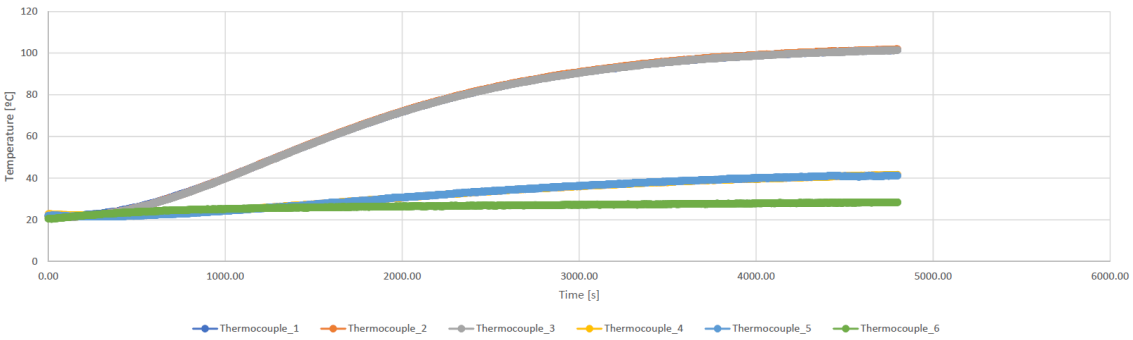

Figure C.2: Ceramic bulb, 50mm separation.

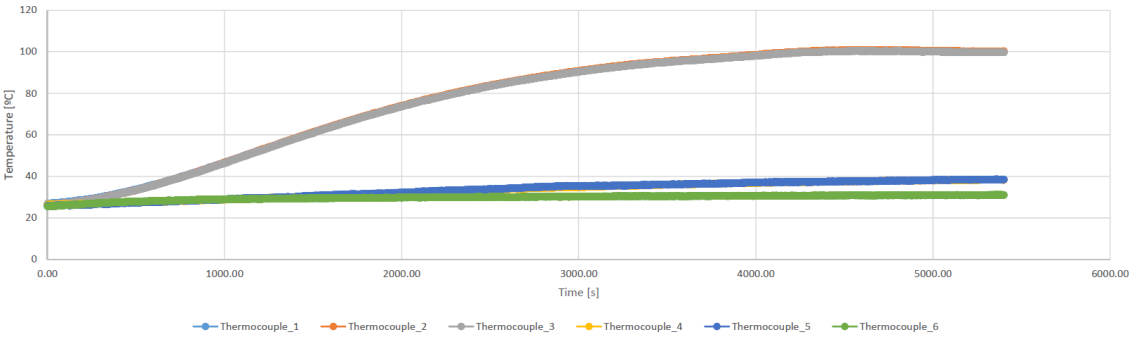

Figure C.3: Ceramic bulb, 100mm separation.

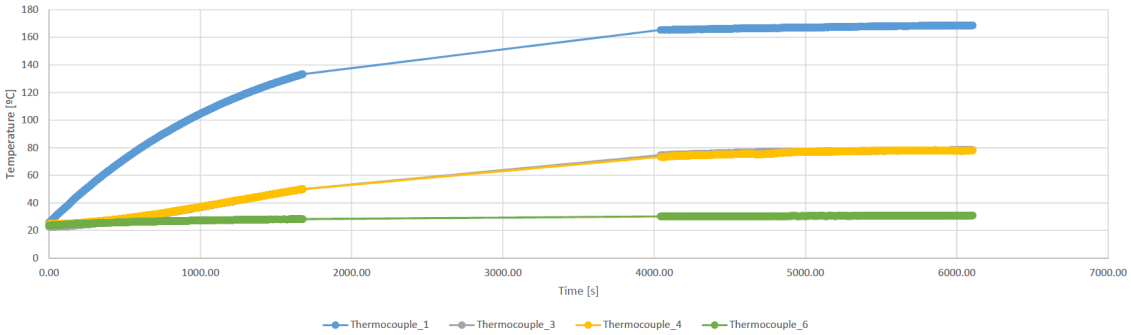

Figure C.4: Incandescent bulb, 20mm separation.

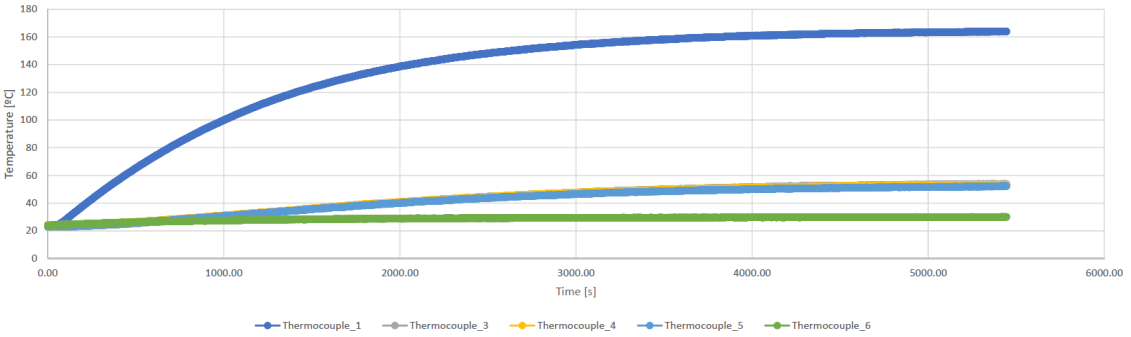

Figure C.5: Incandescent bulb, 50mm separation.

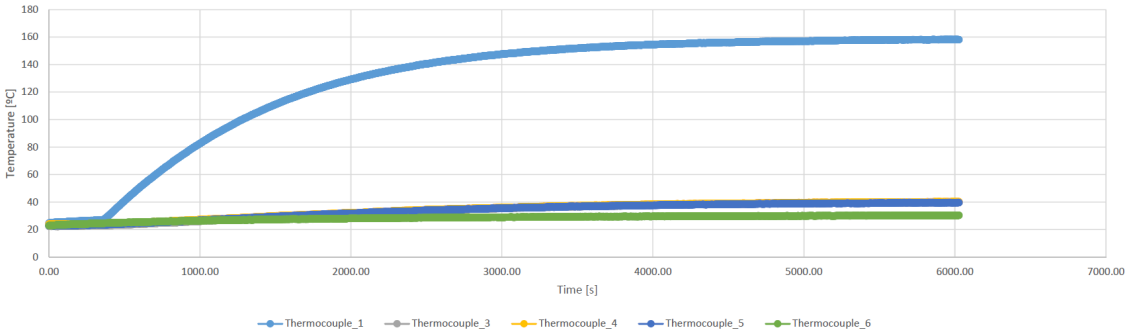

Figure C.6: Incandescent bulb, 100mm separation.

Appendix D

D.1 Experiments Numerical Simulations

This section presents details of experiments modelation in HyperMesh.

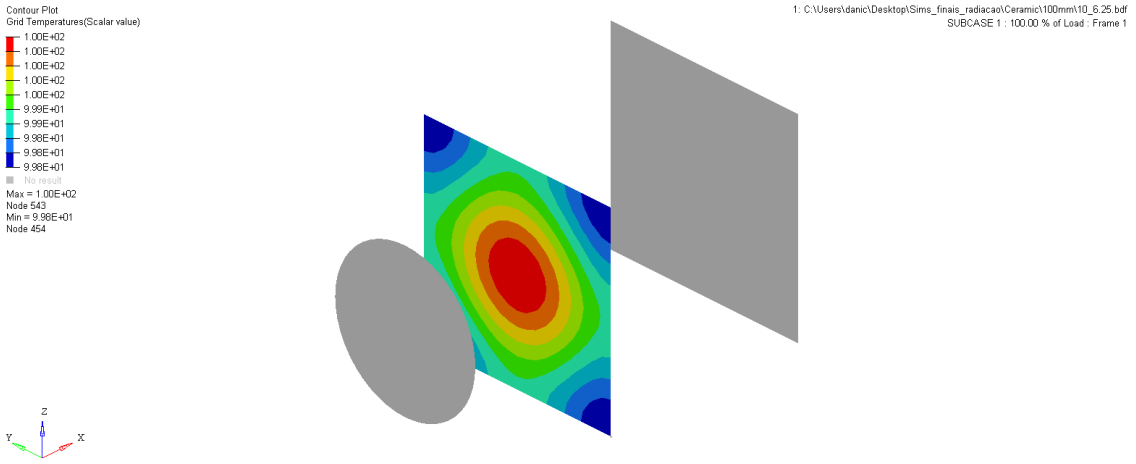

Figure D.1: Numerical results of power estimation analysis.

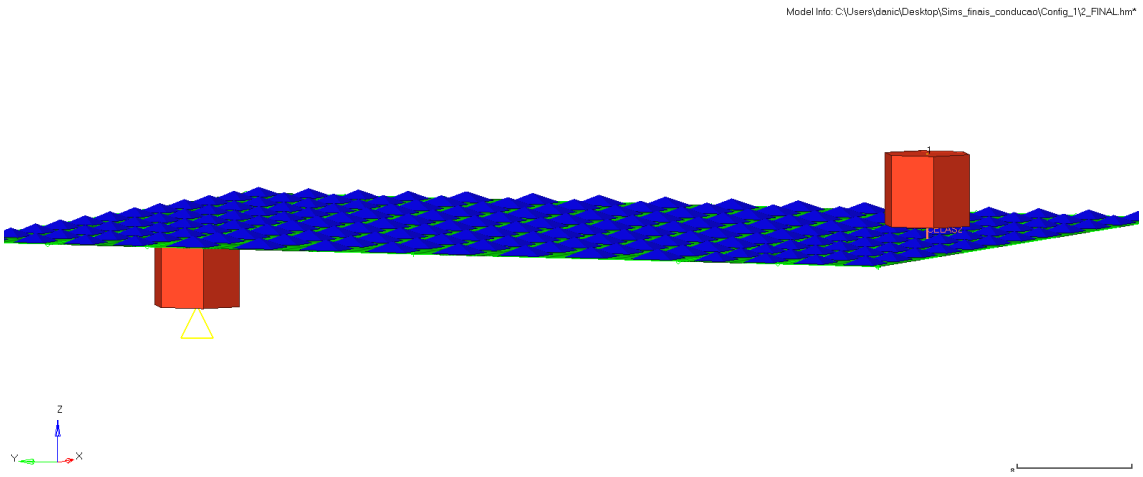

Figure D.2: Thermal conductance model detail.

Appendix E

E.1 CubeSat Model Details

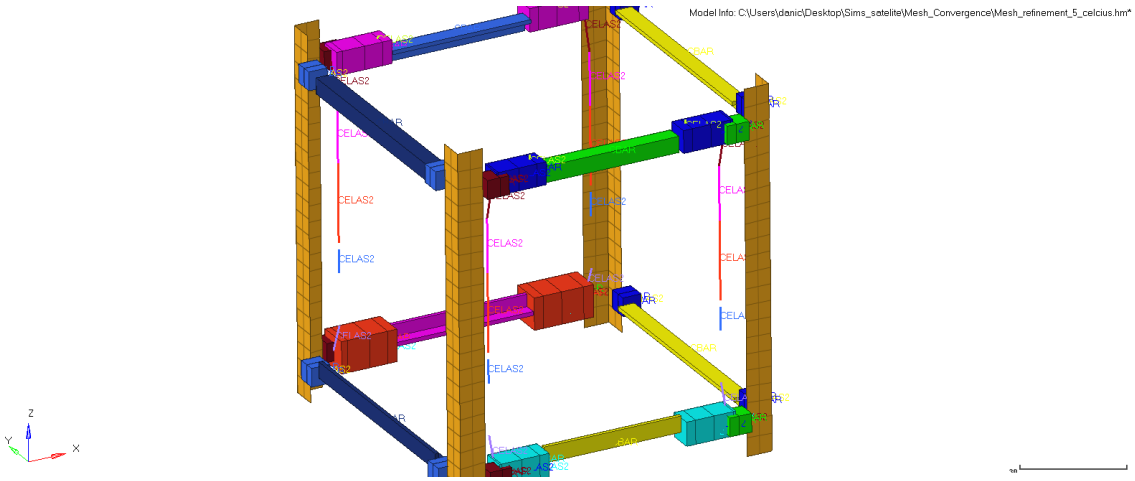

Figure E.1: Satellite structure modeled in HyperMesh.

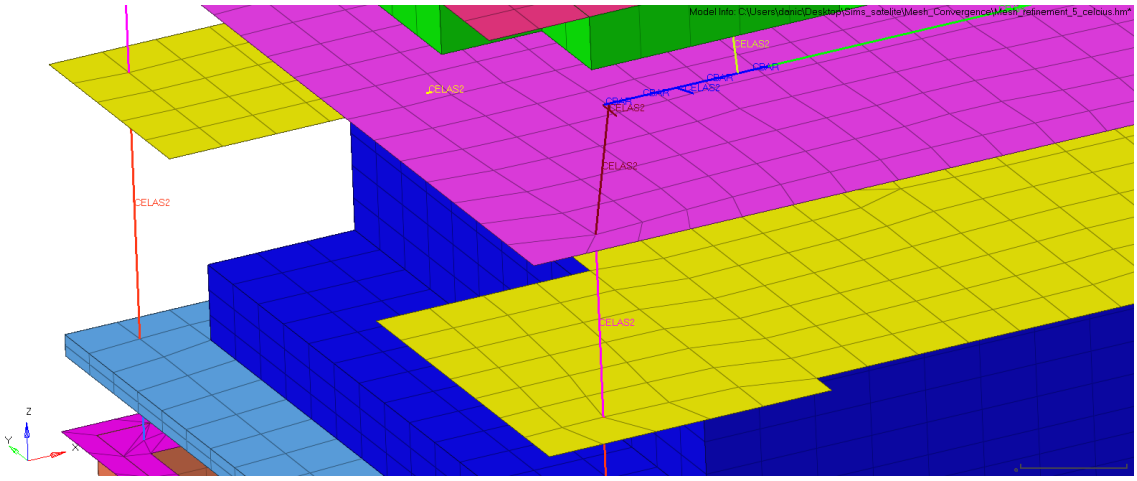

Figure E.2: CubeSat stack connections detail. It is possible to identify CELAS2 elements used to simulate the thermal contact conductance.

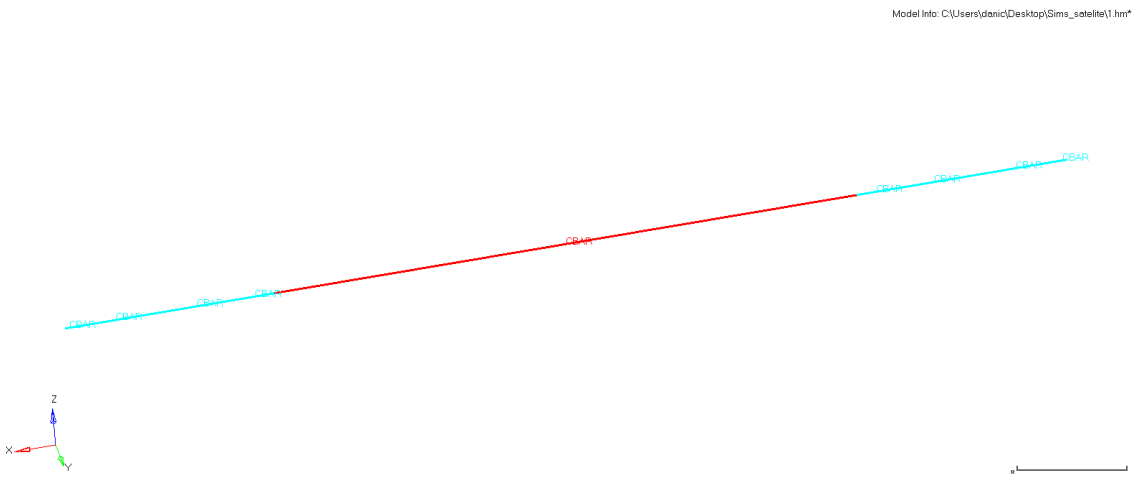

Figure E.3: RIB detail modelation.

E.2 Environment Input Fluxes

Table E.1: Environment input loads used in the thermal model calculated for the orbit considered.

						Environment Input Fluxes	
	Solar Absorptivity	IR Absorptivity	Solar Flux $[W/mm^2]$	Albedo $[W/mm^2]$	IR Earth $[W/mm^2]$	Hot Case	Cold Case
Rails +Y(sun face)	0,14	0,84	0,198	0,000	0,000	0,198	0,000
Rails -Y	0,14	0,84	0,000	0,050	0,164	0,214	0,164
Rails +X	0,14	0,84	0,000	0,015	0,050	0,065	0,050
Rails -X	0,14	0,84	0,000	0,015	0,050	0,065	0,050
Solar Panel +Y(sun face)	0,92	0,85	1,300	0,000	0,000	1,300	0,000
Solar Panel -Y	0,92	0,85	0,000	0,330	0,166	0,496	0,166
Solar Panel +X	0,92	0,85	0,000	0,101	0,050	0,151	0,050
Solar Panel -X	0,92	0,85	0,000	0,101	0,050	0,151	0,050
Antenna Top Plate	0,14	0,84	0,000	0,015	0,050	0,065	0,050
Bottom Plate	0,14	0,84	0,000	0,015	0,050	0,065	0,050
Antenna Side +Y	0,14	0,84	0,198	0,000	0,000	0,198	0,000
Antenna Side -Y	0,14	0,84	0,000	0,050	0,164	0,214	0,164
Antenna Side +X	0,14	0,84	0,000	0,015	0,050	0,065	0,050
Antenna Side -X	0,14	0,84	0,000	0,015	0,050	0,065	0,050

E.3 Thermal Analysis of 3-AMADEUS CubeSat

This section presents details of the results obtained in the thermal analysis of the 3-AAMDEUS CubeSat. Both cases are shown.

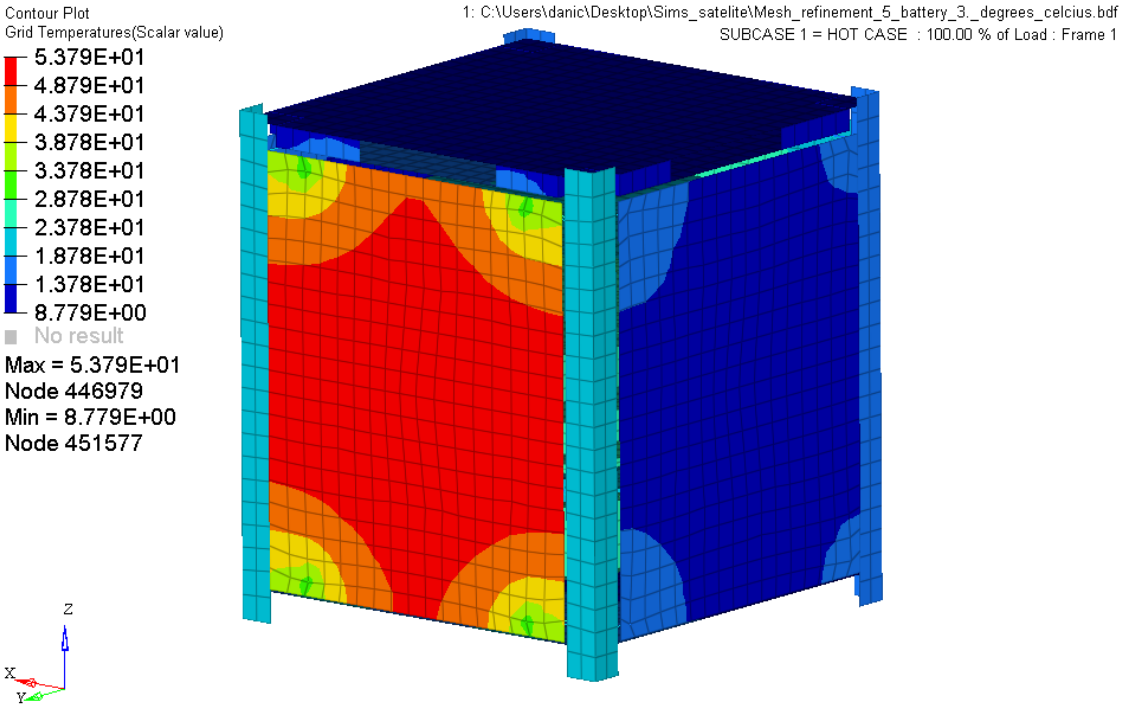

Figure E.4: Hot case results with solar panels.

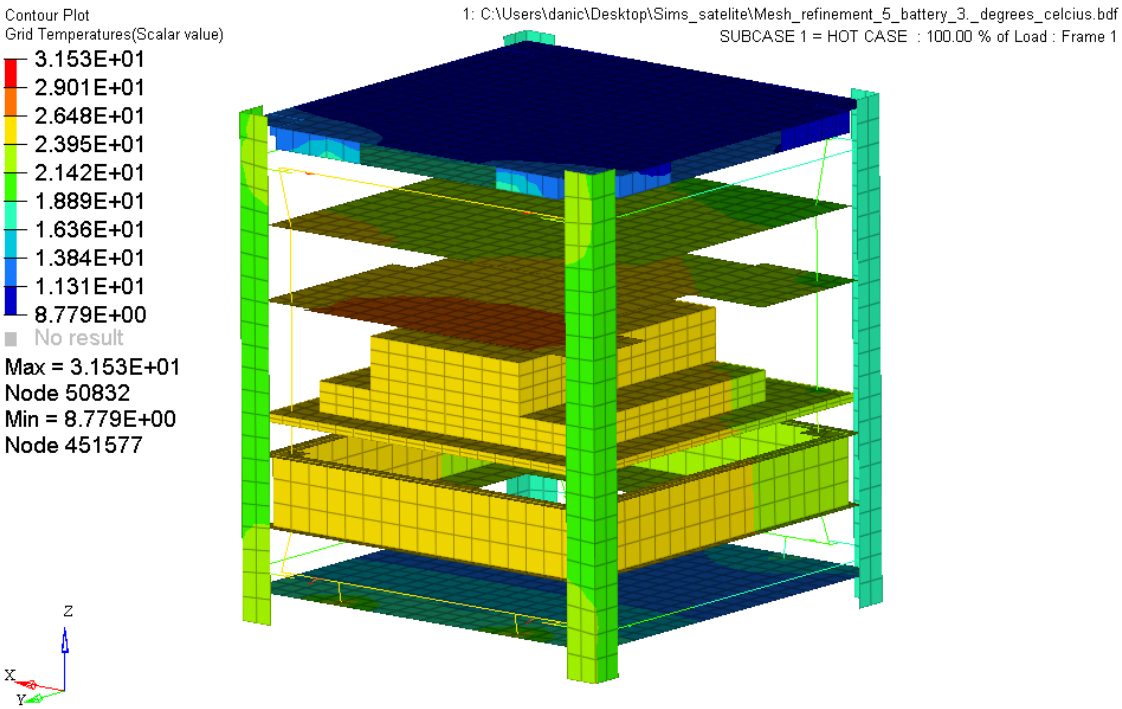

Figure E.5: Hot case results without solar panels.

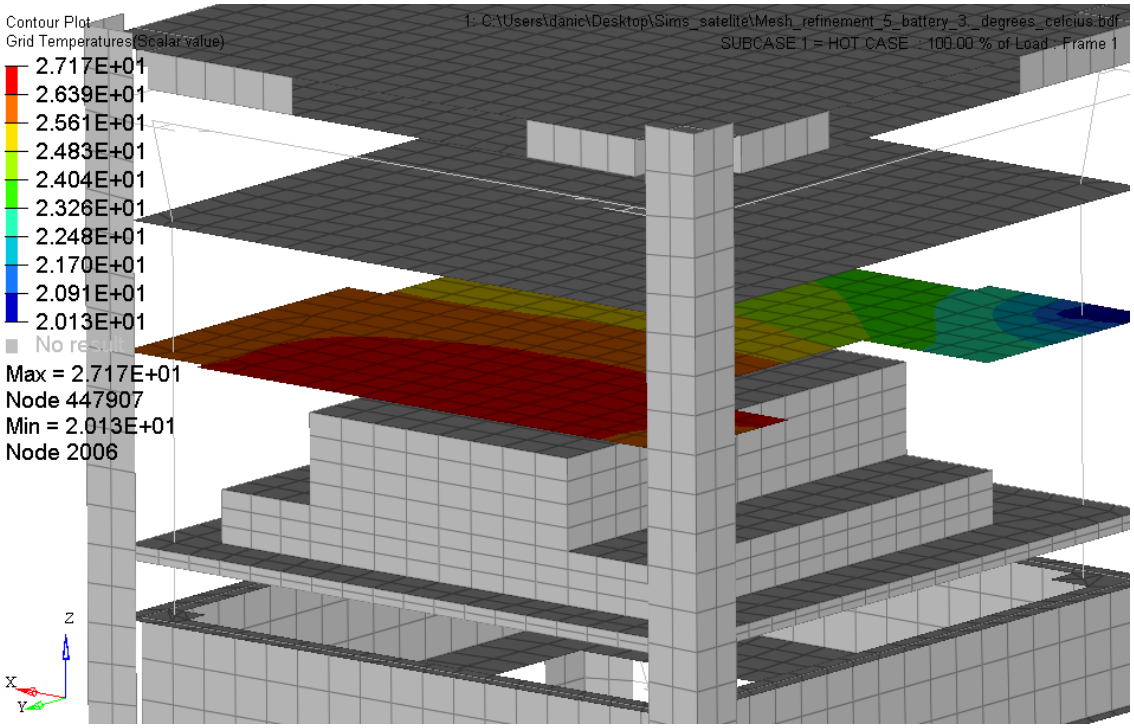

Figure E.6: Temperature distribution of OBC ABACUS, hot case.

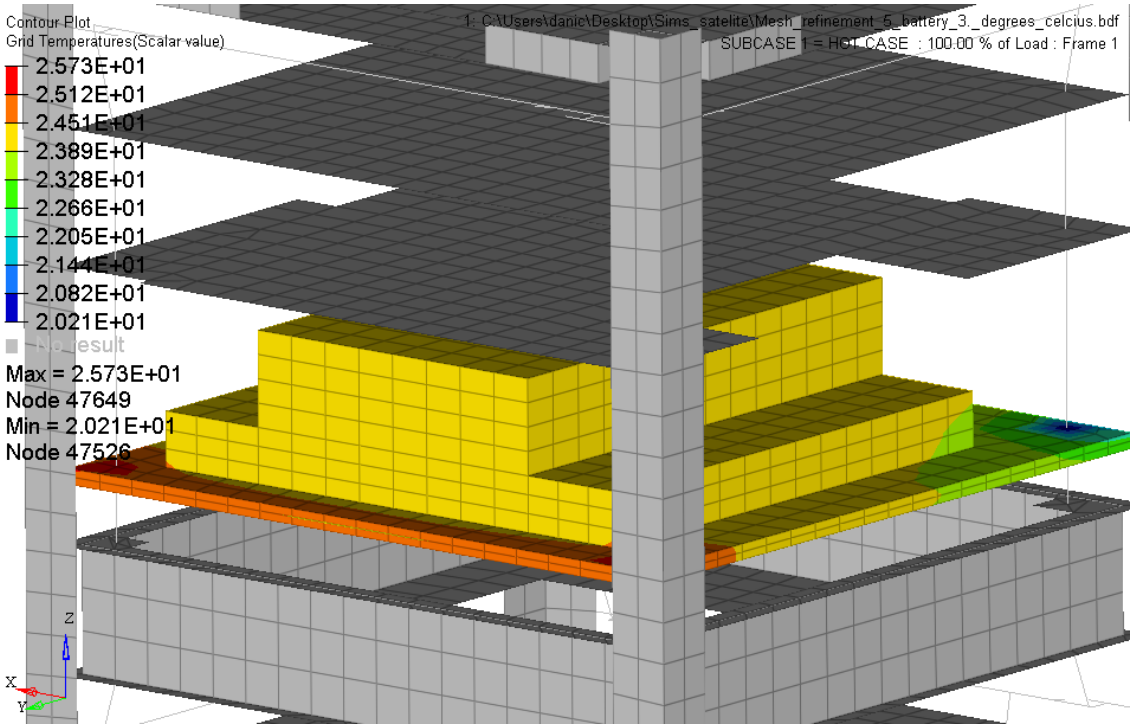

Figure E.7: Temperature distribution of battery, hot case.

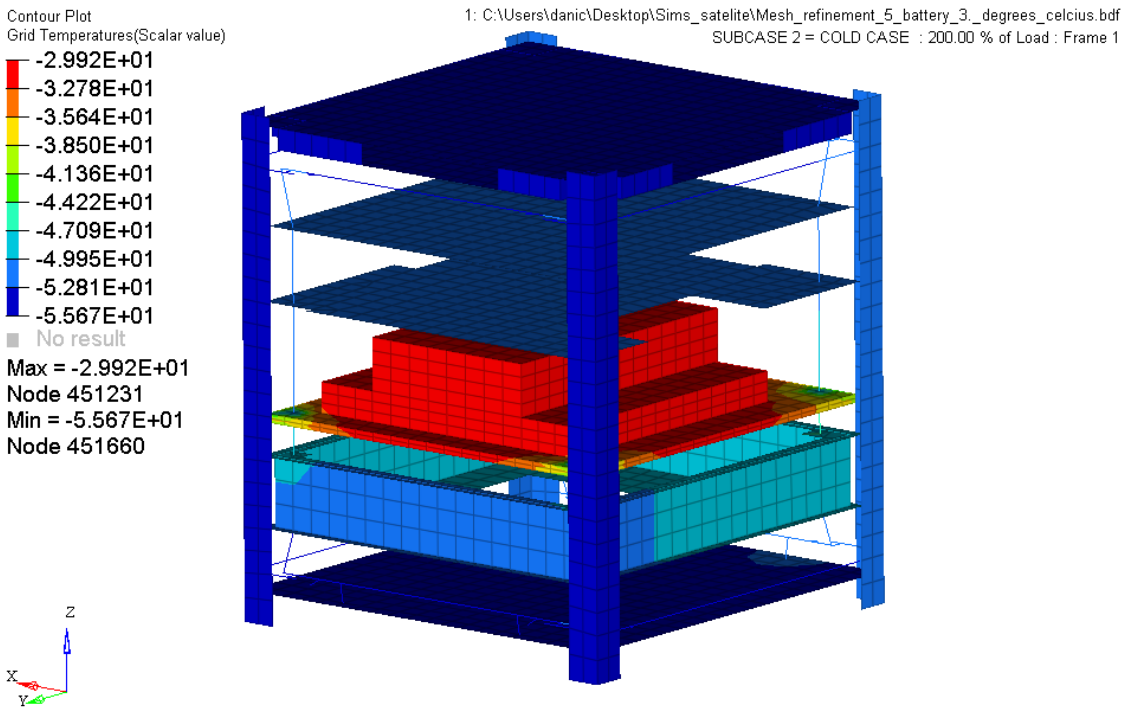

Figure E.8: Cold case results without solar panels.